

Identification of key genes related to the mechanism and prognosis of lung squamous cell carcinoma using bioinformatics analysis

Miaomiao Gao^{a,#}, Weikaixin Kong^{b,#}, Zhuo Huang^{b,*} and Zhengwei Xie^{a,*}

[#]These authors contributed equally to this work

^a*Department of Pharmacology and Department of Biomedical Informatics, School of Basic Medical Sciences, Peking University Health Science Center, 38 Xueyuan Lu, Haidian district, Beijing 100191, China*

^b*Department of Molecular and Cellular Pharmacology, School of Pharmaceutical Sciences, Peking University Health Science Center, 38 Xueyuan Lu, Haidian district, Beijing 100191, China*

* To whom correspondence should be addressed.

ZhengweiXie

Tel: 86-10-82802798; Fax: 86-10-82802798; Email: xiezhengwei@hsc.pku.edu.cn.

Zhuo Huang

E-mail: huangz@hsc.pku.edu.cn

Abstract

Objectives

Lung squamous cell carcinoma (LUSC) often diagnosed as advanced with poor prognosis. The mechanisms of its pathogenesis and prognosis require urgent elucidation. This study was performed to screen potential biomarkers related to the occurrence, development and prognosis of LUSC to reveal unknown physiological and pathological processes.

Materials and Methods

Using bioinformatics analysis, the lung squamous cell carcinoma microarray datasets from the GEO and TCGA databases were analyzed to identify differentially expressed genes (DEGs). Furthermore, PPI and WGCNA network analysis were integrated to identify the key genes closely related to the process of LUSC development. In addition, survival analysis was performed to achieve a prognostic model that accomplished a high level of prediction accuracy.

Results and Conclusion

Eighty-five up-regulated and 39 down-regulated genes were identified, on which functional and pathway enrichment analysis was conducted. GO analysis demonstrated that up-regulated genes were principally enriched in epidermal development and DNA unwinding in DNA replication. Down-regulated genes were mainly involved in cell adhesion, signal transduction and positive regulation of inflammatory response. After PPI and WGCNA network analysis, eight genes, including AURKA, RAD51, TTK, AURKB, CCNA2, TPX2, KPNA2 and KIF23, have been found to play a vital role in LUSC development. The prognostic model contained 20 genes, 18 of which were detrimental to prognosis. The AUC of the established prognostic model for predicting the survival of patients at 1, 3, and 5 years

was 0.828, 0.826 and 0.824, respectively. To conclude, this study identified a number of biomarkers of significant interest for additional investigation of the therapies and methods of prognosis of lung squamous cell carcinoma.

Keywords: lung squamous carcinoma, bioinformatics, prognosis

1. Introduction

Lung cancer is among the deadliest malignancies globally and can be categorized into two main types: small cell lung cancer (SCLC) and non-small cell lung cancer (NSCLC). NSCLC, accounting for approximately 85% of lung cancer cases, is principally divided into lung adenocarcinoma (LUAD) and lung squamous cell carcinoma (LUSC) depending on pathogenesis and histological morphology [1-3]. Many therapeutic methods are currently being used to treat lung cancer, such as surgical resection, chemotherapy, radiotherapy and targeted therapy. Because NSCLC is insensitive to radiotherapy and resistant to anticancer drugs, targeted therapy has become the most effective way to treat patients whose tumors cannot be surgically removed [4,5]. In recent years, targeted therapies have undergone considerable development, and some effective molecular targets have been identified, such as epidermal growth factor receptor (EGFR), anaplastic lymphoma kinase (ALK), *etc.* It has been confirmed that these targets are successful in lung adenocarcinoma, but not in lung squamous cell carcinoma, because the two major subtypes have different mutation profiles [6-8]. In order to better diagnose and treat patients with LUSC, an investigation of novel biomarkers is required. LUSC, which accounts for 30% of cases of NSCLC, is more common in middle-aged and older men and has a high rate of metastasis and recurrence [9]. NSCLC patients are mostly diagnosed during the advanced stage, their 5-year survival rate lower than that of early stage patients [4,10,11]. Thus, further study of prognostic markers is required so as to personalize cancer treatment. Although a number of studies have reported on LUSC-related genes and prognostic markers, the specific molecular mechanisms in the pathogenesis and progression of LUSC have not been systematically evaluated, which constrains the potential for early diagnosis and treatment [12,13]. An in-depth understanding of the molecular mechanisms involved in the occurrence and development of lung cancer may provide a more effective strategy for early detection and subsequent clinical treatment.

Therefore, novel promising biomarkers or potential drug treatments are urgently required.

Genomic microarrays and high-throughput sequencing technology combined with bioinformatics analysis has gradually become a powerful tool for the discovery of disease biomarkers and related pathways. In the present study, three RNA microarray datasets from the GEO database were analyzed to identify differentially expressed genes (DEGs) in lung squamous cell carcinoma compared with normal tissues. Gene ontology (GO) and Kyoto Encyclopedia of Genes (KEGG) analyses were performed to identify key genes and pathways which possibly influence the pathogenesis of LUSC. On the other hand, RNAseq data from the TCGA database were also used to screen out DEGs for weighted gene co-expression network analysis (WGCNA) so as to obtain hub genes associated with the occurrence and development of LUSC. Eventually, key genes at the intersection of these two databases identified genes that are critical to the disease. In addition, we utilized patient clinical information from DEGs in the TCGA for univariate cox regression analysis, lasso regression analysis and multivariate cox regression analysis to identify prognostic-related key genes. This ensured that an improved understanding of the mechanism and prognosis of lung squamous cell carcinoma was obtained.

2. Material and methods

2.1 Data Collection and data processing

The Gene Expression Omnibus (GEO, <https://www.ncbi.nlm.nih.gov/geo/>) database from the National Center for Biotechnology Information was searched for publicly available studies and samples that fulfilled the following criteria for analysis: (1) the gene expression data series contained LUSC tissue and normal tissue samples; (2) the species of the samples was Homo Sapiens. Finally, three gene expression profiles (GSE2088, GSE6044, GSE19188) were collected for further analysis [14]. These three datasets were downloaded, the details of

which are shown in Sup.Table 1. GEO2R was used to calculate the fold change value and P-values of every gene in each group. Any gene for which $|\log_2FC| > 1$ and P-value < 0.05 was defined as a differentially expressed gene [15]. If multiple probes corresponded to the same gene, the maximum value of fold change was considered the gene expression level.

2.2 TCGA data validation

To ensure accuracy, further validation analysis was performed to confirm the results. LUSC RNAseq data was downloaded from The Cancer Genome Atlas (TCGA, <https://www.cancer.gov/tcga>) database, acquired using the Illumina HiSeq platform. The dataset included 502 LUSC samples and 49 normal samples. The genomic data used was standardized using the fpkm method [16]. For repetitive genetic data, the largest value was utilized as the expression level. Genes with a mean expression of less than 0.5 were excluded in each case to ensure significantly expressed genes were evaluated. The p-values of differentially-expressed genes were identified using a Wilcox test. From analysis methods of the GEO data, DEGs in the SCC samples compared with normal samples were identified. Raw P-values obtained from the Wilcox test and \log_2FC calculation were adjusted using the BH16 method [17]. Thresholds of $|\log_2FC| > 1.0$ and an adjusted P-value of < 0.05 were selected. The process above was conducted using the R package "limma".

2.3 Functional and pathway enrichment analysis

The GO database has a large collection of gene annotation terms, allowing genome annotation using consistent terminology. GO enrichment analysis including molecular function, cellular components and biological processes, identified which GO terms were over or underrepresented within a given set of genes [18]. The KEGG knowledge database, an integrated database resource, is generally used to identify functional and metabolic pathways [19]. GO and KEGG analysis were both conducted using the Database for Annotation, Visualization and Integrated Discovery (DAVID, <https://david.ncifcrf.gov/>), analysis tools for

extracting meaningful biological information from multiple gene and protein collections [20,21]. Up- and down-regulated genes were analyzed separately, a P-value < 0.05 considered the threshold value.

2.4 PPI network construction and analysis of modules

Protein-protein interaction (PPI) networks can assist in identifying key genes and pivotal gene modules involved in the development of LUSC from an interaction level. The Search Tool for The Retrieval of Interaction Genes (STRING, <https://string-db.org/>) was used to construct PPI networks. STRING is a database which provides critical assessment and integration of protein–protein interactions, including physical and functional associations [22]. DEGs were mapped to STRING to evaluate the PPI information and set confidence score > 0.4 as the cut-off standard. Cytoscape was used to visualize the PPI network, a practical open-source software tool for the visual exploration of biomolecule interaction networks consisting of protein, gene and other types of interaction [23]. Module analysis was conducted using the plug-in Molecular Complex Detection (MCODE) in Cytoscape to display the biological significance of gene modules [24].

2.5 Weighted correlation network analysis of DEGs

In the WGCNA algorithm [25], the power exponential weighting of gene correlation coefficients was used to represent the correlation between genes. The power value β was selected such that connections between genes were subject to scale-free network distribution. A topological matrix that incorporated surrounding genetic information was calculated relative to distance d .

$$S_{ij} = \text{cor}(i, j)$$

$$\alpha_{ij} = |S_{ij}|^{\beta}$$

$$\omega_{ij} = \frac{l_{ij} + \alpha_{ij}}{\min\{k_i, k_j\} + 1 - \alpha_{ij}}$$

$$d_{ij} = 1 - \omega_{ij}$$

where $l_{ij} = \sum u \alpha_i u \alpha_j$ and $k_i = \sum u \alpha_i u$ represented node connectivity. The samples were firstly clustered using hierarchical clustering and the threshold set to 40,000 to eliminate outliers. d was then calculated and the dynamic pruning method was used after determining values of gene module parameters (maxBlockSize=7000, deepSplit = 2, minModuleSize = 80, mergeCutHeight = 0.25). After obtaining these, Pearson correlation coefficients of the gene modules and phenotypes (cancer tissue or paracancerous tissue samples) were calculated. This allowed selection of gene modules closely related to tumorigenesis. Genes in the gene modules from GO and KEGG analysis were used to observe the function of each gene module. Next, two indicators for the genes in these gene modules were calculated: one was the Pearson correlation coefficient of the gene in the module and the first principal component of the module, termed Module Membership (MM); the other is the Pearson correlation coefficient of the gene and phenotype in the sample, termed Gene Significance (GS). If a gene within a module had both large MM and GS, then the gene was considered to be a key gene in the module. In this study, genes in which the MM and GS were in the upper quartile of all genes in the module were identified as key genes. The key genes in key modules (modules with a high correlation coefficient for phenotype) were compared with key genes derived from PPI to obtain decisive genes in the development of LUSC. The WGCNA calculations were accomplished using the "WGCNA" package in R [26].

2.6 Survival analysis

Patient clinical data were downloaded from the TCGA website, then samples missing overall survival (OS) data were deleted, finally resulting in a total of 493 samples for survival analysis. Univariate Cox proportional hazards regression analysis was used to screen for

genes significantly associated with prognosis ($P < 0.05$) [27]. Later, lasso regression analysis was used to eliminate collinearity between genes. After performing 1000 10-fold cross-validations, the λ value in which the error was minimized was selected as the optimum λ parameter value [28]. Then multivariate Cox proportional hazards regression analysis was used to find key genes involved in the establishment of a prognostic model [29]. The model used disease risk scores as predictors of prognostic status. The disease risk score was determined by parameter β of the multivariate Cox proportional hazards regression analysis and the magnitude of the expression of each gene in the sample, using the following formula:

$$\text{Risk score} = \sum_{i=1}^N \text{Exp}_i \times \beta_i$$

where Exp_i and β are the expression levels of gene i in a particular patient and coefficients of the gene i in the multivariate cox regression analysis [30]. The risk score for each patient was calculated, which were then categorized into high or low-risk in comparison with the median value. Kaplan-Meier survival curves were then plotted to evaluate whether the prediction effect of the model was significant ($p < 0.05$). The statistical method used in this process was a Log-rank test. The predictive performance of this model at different endpoints (1, 3 or 5 years) was assessed using a time-dependent receiver operating characteristic (ROC) curve [31]. The R packages used in the survival analysis procedure included: "survival", "caret", "glmnet", "survminer" and "survivalROC".

3. Results

3.1 Identification of DEGs

Prior to GEO2R analysis, hierarchical clustering was employed to detect sample groups and remove data deviating from the sample group. After measuring the quality of samples, in total there were 97 normal lung samples and 84 with LUSC. Finally, a total of 1013, 675 and

3398 DGEs were identified from the three datasets. Among these DEGs, 128 genes were found in all three sets, including 88 significantly up-regulated DEGs and 4 significantly down-regulated DEGs. In a TCGA dataset containing 49 normal samples and 499 LUSC samples, 3348 up-regulated genes, 3387 down-regulated genes were identified (information on DEGs of the three GEO and one TCGA datasets and the overlap of genes between the datasets is displayed in Supplementary Table). The intersection is shown in Figure 1, including 85 significantly up-regulated and 39 down-regulated genes, the change in direction of expression of TCGA consistent with the DEGs in the GEO database. These genes were used to perform subsequent functional and pathway enrichment analysis.

3.2 GO term and KEGG pathway enrichment analysis of DEGs

The function and mechanism of the DEGs identified in this way were further evaluated by GO term and KEGG pathway analysis. Up- and down-regulated genes were uploaded to DAVID to conduct the analysis. In biological processes, up-regulated DEGs were significantly associated with epidermis development, collagen catabolic process, collagen fibril organization. Down-regulated DEGs were predominantly involved in cell adhesion, signal transduction, positive regulation of inflammatory response and regulation of cell growth. For molecular function, significantly up-regulated DEGs were represented by response to protein binding, and structural molecular activity while significantly down-regulated DEGs were involved in flavin adenine dinucleotide binding, thrombospondin receptor activity, and protein binding. For cellular components, significantly up-regulated DEGs were enriched in cytosol, extracellular matrix, desmosome and those that were significantly down-regulated were found in extracellular exosome and space, and membrane raft. Figure 2 presents additional details regarding GO term analysis. In addition, KEGG pathway analysis identified six enriched pathways, in which three were over-represented in up-regulated genes, including cell cycle, ECM-receptor interaction, and amoebiasis. Down-

regulated genes enriched in three metabolic pathways, namely drug metabolism of cytochrome P450, tyrosine metabolism and phenylalanine metabolism (Sup. Table 2).

3.3 PPI network analysis of DEGs

The PPI network was constructed by Cytoscape based on the STRING database, consisting of 105 nodes and 483 edges, including 76 up- and 29 down-regulated genes (Figure 3A). The 15 DGEs with the greatest degree of connectivity were selected as key genes of SCC. These genes were: RFC4, AURKA, MAD2L1, TPX2, CCNA2, AURKB, TTK, TOP2A, RAD51, CDKN3, TK1, KPNA2, KIF23, PBK and UBE2C, which may play an important role in SCC progression. MCODE in Cytoscape was used to perform module analysis. Four significant modules were identified after MCODE analysis. The most significant module (MCODE score = 23.217) included 24 nodes and 267 edges (Figure 3B). Remarkably, genes in this module were all up-regulated. Functional and pathway enrichment analysis of the DEGs in this module were also conducted using DAVID. GO term enrichment analysis demonstrated that genes in this module were principally enriched in cell division and mitotic nuclear division in biological processes. Cell component analysis indicated that genes were significantly enriched in nucleoplasm, spindle and kinetochore. Molecular functional analysis demonstrated that the genes were principally involved in the binding of ATP and protein. KEGG analysis suggested that the genes were mainly involved in cell cycle (Table 1). The other three modules were shown in Sup. Figure 1.

3.4 Weighted gene correlation network analysis of DEGs

Based on the results of hierarchical clustering, we first removed two samples: TCGA.63.5128.01 and TCGA.92.8065.01 (Sup. Figure 2). A value of $\beta=5$ was selected as a soft threshold to establish a gene regulatory network (Figure 4A). After obtaining the gene modules using a dynamic pruning method, it was found that the correlation coefficients of the blue, yellow and turquoise modules were greatest, at 0.538, -0.542 and -0.870, respectively

(Figure 4C). In addition, the first principal component of the genes in these modules and the Pearson correlation coefficient between the modules in terms of clustering, were calculated. From these results (Figure 4B), we can see that the three modules turquoise, yellow and red were of greatest consistency. The correlation coefficients of these three modules and phenotypes were negative. The GO and KEGG analysis results for the blue, yellow and turquoise modules are shown in Sup. Figure 3. It can be seen that the genes in the yellow module were more related to inflammatory and immune response processes, also a key module most likely to appear in the WGCNA analysis of other disease and control groups [32]. The blue module was more closely related to cell cycle, mitosis, chromosome structure changes, etc., possibly related to the excessive proliferation of cells during cancer, targeted by many classic anticancer drugs such as paclitaxel and vinblastine [33,34], that play important roles in these processes. Thus, genes in this module are important for drug development. The results of GO and KEGG analysis of the turquoise module were more complex. This principally included cell migration and adhesion, response to hormones, tissue development, cell-growth pathway (TGF-beta signaling pathway, etc.), and immune processes. Among the 20 key genes obtained by PPI, 8 genes were located in the blue module and belonged to key genes of the blue module (Sup.Table 3), while the other 11 genes were not present among key genes of any module.

3.5 Survival analysis

In order to establish an effective model for predicting prognostic status, univariate Cox proportional hazards regression analysis was used, with Lasso regression analysis and multivariate Cox proportional hazards regression analysis to screen genes. In the Univariate Cox proportional hazards regression analysis, 111 genes with significant effects on prognosis ($p < 0.01$, Supplementary Table) were identified. In lasso regression, following 10-fold cross-validation with 1000 repeats, λ was 0.0007079 (Figure 5D), where Partial Likelihood

Deviance was smallest. For a λ of this value, 33 of the 111 genes had coefficients that were not zero (Figure 5E). A total of 20 genes were obtained by the forward-backward selection technique in multivariate Cox proportional hazards regression analysis for to establish a prognostic risk score model, namely: KLK8, POPDC3, IGLL1, PLEKHA6, PTGIS, ANKFN1, TM4SF19, JAG1, OR2W3, RALGAPA2, RPH3AL, PCDHGA7, C10orf55, ACPT, MMP12, H1FOO, CT45A10, UGT2A1, a low expression of which improved prognosis, and LYSMD1 and ONECUT3, where improved prognosis occurred with high expression (Figure 6A).

$$\begin{aligned} \text{Risk score} = & (0.00943 \times \text{KLK8}) + (0.01536 \times \text{POPDC3}) + (0.04825 \times \text{IGLL1}) + \\ & (-0.04272 \times \text{LYSMD1}) + (0.01822 \times \text{PLEKHA6}) + (0.01318 \times \text{PTGIS}) + (0.14178 \times \\ & \text{ANKFN1}) + (0.02925 \times \text{TM4SF19}) + (0.00116 \times \text{JAG1}) + (0.11625 \times \text{OR2W3}) + \\ & (-0.47624 \times \text{ONECUT3}) + (0.01810 \times \text{RALGAPA2}) + (0.03305 \times \text{RPH3AL}) + (0.06967 \\ & \times \text{PCDHGA7}) + (0.06217 \times \text{C10orf55}) + (0.08721 \times \text{ACPT}) + (0.00082 \times \text{MMP12}) + \\ & (0.58094 \times \text{H1FOO}) + (0.01348 \times \text{CT45A10}) + (0.02889 \times \text{UGT2A1}). \end{aligned}$$

The distribution of risk scores and groupings are shown in Figure 5A. Patient risk scores are ranked and patient gene expression plotted as a heatmap (Figure 5C). It can be seen from the heat map that gene expression levels with a negative coefficient gradually decreased as risk score increased. Conversely, expression levels of genes with a positive coefficient displayed the opposite. As risk scores increased, the number of patients that died increased and duration of survival gradually decreased, confirming that the risk model was realistic (Figure 5B). The Kaplan–Meier curves were grouped by defined risk scores. It can be seen that prognosis of the low-risk group was significantly better than that of the high-risk group (Figure 5F). By predicting survival of patients at 1, 3, and 5 years, the area under the curve

(AUC) of the ROC curves obtained from the risk-based prediction model was 0.828, 0.826 and 0.824 (Figure 6B).

4. Discussion

Although many relevant studies of LUSC have been performed, early diagnosis, efficacy of treatment and prognosis for LUSC remain poorly resolved. For diagnosis and treatment, it is necessary to further understand the molecular mechanisms resulting in occurrence and development. Due to the development of high-throughput sequencing technology, the genetic alterations due to disease progression can be detected, indicating gene targets for diagnosis, therapy and prognosis of specific diseases.

In this study, the intergrading of GEO and TCGA data for LUSC resulted in the identification of 124 significantly DEGs in lung squamous cell cancer compared with normal samples, including 85 up-regulated DEGs and 39 that were down-regulated. GO analysis demonstrated that the up-regulated genes were principally involved in epidermal development and DNA unwinding in DNA replication, while the down-regulated genes were mainly enriched in cell adhesion, signal transduction and positive regulation of inflammatory response. KEGG analysis indicated that these differentially expressed genes were involved in cell cycle regulation, cancer-related pathways, ECM receptor interaction and various metabolic pathways. In addition, 15 genes of high significance, including RFC4, AURKA, MAD2L1, TPX2, CCNA2, AURKB, TTK, TOP2A, RAD51, CDKN3, TK1, KPNA2, KIF23, PBK and UBE2C, were identified by constructing a PPI network. Through module analysis we identified four significant gene modules, in which the most significant module contained 26 nodes and 267 edges strongly associated with cell division and related activities. Interestingly, the genes in this module were all up-regulated and fifteen key genes of the highest significance were contained in this module. Through WGCNA analysis, three

significant gene modules, in which the blue module was positively correlated with the development of tumors, the opposite of the others, were obtained. Key genes identified in the PPI network were mostly contained in the blue module, including AURKA, RAD51, TTK, AURKB, CCNA2, TPX2, KPNA2 and KIF23. GO analysis indicated that the blue module was associated with cell cycle, consistent with PPI submodule analysis. The WGCNA package constructed a network based on the correlation between genes, whereas the PPI network was based on protein networks reported in the known literature. It seems appropriate to combine WGCNA and PPI methods to identify key genes. Thus, these eight genes were selected as hub genes for the occurrence and development of LUSC. All eight are involved in cell cycle progression and regulate different mitotic events. A large number of studies have reported that abnormal expression levels were found in multiple types of human malignancy and have potential as anticancer therapeutic targets [35-40].

AURKA and AURKB are members of the aurora kinase family and both play central roles in regulating cell-cycle progression from G2 through to cytokinesis. AURKA is involved in many mitotic events, including centrosome maturation, mitosis entry, mitotic spindle formation and cytokinesis [41]. AURKB exerts its function by regulating chromosomal alignment, segregation and cytokinesis, as the catalytic protein of the chromosomal passenger complex (CPC) [40]. Yu *et al.* identified functional interaction between AURKA and AURKB, assisting in protection of their stability and partially explaining their persistent high expression and activity in cancers [43]. Ma *et al.* verified that up-regulation of miR-32 down-regulated AURKA and thus inhibited the occurrence and development of NSCLC [44]. Jin *et al.* performed a bioinformatics analysis and proposed that AURKB may be the key gene in LUAC and could result in poor prognosis [45].

RAD51 is the central protein in the homologous recombination (HR) pathway and is critical for DNA replication and repair. Recent studies have reported that RAD51 is also

implicated in the suppression of innate immunity [46]. Hu *et al.* pointed out that RAD51 expression was elevated by a KRAS mutation which predominantly occurred in lung adenocarcinomas. Furthermore, they found that the high expression of RAD51 was associated with poor survival in lung adenocarcinoma through analysis of data from the TCGA database [47]. Moreover, expression levels of RAD51 were also linked to resistance to chemotherapy. Takenaka *et al.* reported that the combined expression of RAD51 and another DNA repair enzyme, ERCC1 (Excision repair cross-complementation group 1) is associated with resistance to platinum agents, indicating the potential role of RAD51 in prognosis [48].

Monopolar spindle1 (Mps1), also known as TTK, is a dual-specificity kinase that phosphorylates serine/threonine and tyrosine residues. TTK is a key mitotic checkpoint protein, similar to AURKA and AURKB. It functions as a critical component of the SAC (spindle assembly checkpoint) signaling cascade, ensuring correct chromosome segregation [49]. High expression of TTK in LUAC and LUSC has been revealed through analysis of TCGA data, where it eliminates lung cancer by augmenting apoptosis and polyploidy [50]. Cyclin family member CCNA2 is involved in cytoskeletal dynamics, epithelial–mesenchymal transition (EMT) and metastasis [51]. Chen *et al.* used two lung adenocarcinoma cell lines to verify that miR-137 can induce G1/S cell cycle arrest and dysregulate mRNA expression in cell cycle associated proteins, including CCNA2 [52].

TPX2, a microtubule-associated protein, is required for the formation of normal bipolar spindles and chromosome separation. Overexpression of TPX2 can induce abnormal centrosome amplification, leading to aneuploidy formation and malignant transformation of cells. It can also promote cell proliferation and participate in cell cycle and apoptosis regulation [53]. It is overexpressed in LUSC, which has been specifically verified [54]. Remarkably, TPX2 can specifically interact with AURKA to complete a series of biological

functions including targeting of AURKA to the spindle microtubules and assembly of spindles of the correct length which faithfully segregate chromosomes [55]. Co-expression of TPX2 and AURKA have been verified, depletion of either causing defects in the formation of spindles [35,55]. In LUSC, up-regulation of AURKA and TPX2 are correlated, a high correlation in tumor tissues having been established [56].

KPNA2 regulates the transportation of a variety of important proteins from the cytoplasm into the nucleus. Increasing evidence has shown that KPNA2 contributes to the process of gene regulation, including that of oncogenes and tumor-suppressor genes, further affecting biological functions, such as cell proliferation, differentiation, cell-matrix adhesion, colony formation and migration [57]. Wang *et al.* found that KPNA2 was overexpressed in the nuclei of tumor cells in NSCLC, through analysis of the cancer cell secretome and tissue transcriptome, suggesting that KPNA2 is a potential biomarker for NSCLC [58].

Nuclear protein KIF23 is reported to interact with the aurora kinase family to regulate cell division and cytokinesis [59]. A reduction in KIF23 gene expression was able to suppress cell proliferation [60]. A number of experimental and bioinformatics studies have pointed to high levels of KIF23 expression observed in the majority of metastatic lung cancer tissues, indicating that KIF23 plays a role in NSCLC occurrence and development [36,61-63]. Importantly, abnormal behavior of genes in lung cancer has been widely reported. However, its role and molecular mechanisms in LUSC require additional investigation.

We have established a prognostic model that predicts patient survival. This model contains 20 key genes, some of which have not been reported in the literature in LUSC studies, including POPDC3, IGLL1, TM4SF19, RALGAPA2, RPH3AL, PCDHGA7 or ACPT. The present study found that KLK8 (kallikrein8) is involved in the development of a variety of tumors, including cervical, ovarian and breast cancer. KLK8 is expressed in different tissues and cells and regulated by steroid hormones [64-66]. KLK is distributed

principally in normal tissues such as the kidneys, breast, skin, tonsil, testis, *etc.*, but KLK8 is expressed less in the lungs, which may be a reason for the small coefficient (0.00943) for KLK8 in the risk score [67]. That study demonstrated that KLK8 is highly expressed in ovarian cancer and can be used as a marker for tumorigenesis. Whether KLK8 can be used as a biomarker for squamous cell carcinoma deserves further investigation [68]. High expression of LYSMD1 and ONECUT3 has a protective effect on squamous cell carcinoma. LYSMD1 is a member of the LysM domain. The LysM domain is widely found in plants, bacteria, fungi and animals [69,70] and can be combined with a variety of other proteins. At present, few studies have reported on its role in mammalian tissues, but it can be seen from the results of survival analysis that high expression of LYSMD1 may have a protective effect on keratinized squamous cell carcinoma.

The ONECUT transcription factor contains three members in mammalian cells, namely hepatocyte nuclear factor 6 (ONECUT-1), ONECUT-2 (OC-2) and ONECUT-3 (OC-3), roles of which overlap [71]. ONECUT participates in the biological functions of cell cycle and proliferation regulation, cell differentiation, organ formation, cell migration, cell adhesion and metabolism by regulation of gene expression [72]. Current studies on the regulation of cell proliferation by OC transcription factors are focusing mainly on ONECUT-1. It is worth noting that ONECUT-1 has a certain tissue specificity for the regulation of cell proliferation. For example, overexpression of ONECUT-1 in colonic adenocarcinoma cell line Caco-2 inhibits cell cycle progression [73]. At present, there are few reports of the regulation of cell cycle in ONECUT-3, but the high expression of this gene has a significant prognostic effect. In lung tissue, the expression of ONECUT-1 is reduced, so ONECUT-3 may regulate cell cycle and adhesion, but this requires further experimental verification. Related studies have shown that the occurrence of lung cancer and the metastasis of cancer cells can significantly change the patient's olfactory function, consistent with the genes we have identified. Thus,

OR2W3 (olfactory receptor family 2 subfamily W member 3) could potentially be used as a tumor marker for the examination of squamous cell carcinoma [74,75].

H1FOO is an H1.8 linker histone. Expression levels of this gene are closely related to time course, but different from other H1 protein subtypes. It not only functions in oocyte-embryo development transition, but also plays a crucial role in the genome reprogramming process. When the expression of the H1FOO gene in oocytes increases, the pluripotency of the cells also increases, indicating that H1FOO is involved in chromosome remodeling and gene reprogramming. This process is closely related to the occurrence of cancer, so to some extent, the levels of H1FOO expression reflect the degree of cancer cell proliferation [76,77].

Ankyrin repeats play an important role in the progression of inflammation-associated tumors. At present, it has been found that ankyrin repeats are highly expressed in cervical cancer, liver cancer, cholangiocarcinoma, breast cancer, *etc.* and that their expression levels are closely related to depth of tumor invasion, grading stage [78] and tumor metastasis. Studies have suggested that ankyrin repeats may play a role in cell proliferation by regulating the function of the important tumor suppressor genes p53, Rb and hypoxia inducible factor-1 (HIF-1), and the IL-8 pathway [79]. The protein fibronectin is a glycoprotein secreted by tumor-associated fibroblasts and tumor cells. Deposition of fibronectin stimulates cancer cells to bind to insulin-like growth factor binding protein-3 (IGFBP-3) and epidermal growth factor (EGF) [80]. When fibronectin increases in concentration, IGFBP-3 and EGF promote cancer cell proliferation. Conversely, if fibronectin is deleted, cancer cell proliferation is inhibited. This is consistent with the large positive coefficient (0.14178) for the ANKFN1 (ankyrin repeat and fibronectin type III domain containing 1) gene obtained in the present study.

5. Conclusions

In the present study, microarray data from the GEO database were integrated with RNA sequencing data from the TCGA, to identify key genes and more important hub genes. Finally, we identified eight hub genes associated with the pathogenesis and progression of LUSC. Additionally, we performed survival analysis and built a Cox proportional hazards model to identify prognostic biomarkers. A prognostic gene signature consisting of 20 genes was constructed with good performance in predicting overall survival. These results will serve as a reference for future research on the pathogenesis and drug treatment for LUSC. Nevertheless, the lack of experimental verification is a limitation of this study. The predictions obtained from the bioinformatics analysis can be verified by future experimental studies.

Data availability

Gene Expression Omnibus (GEO, <https://www.ncbi.nlm.nih.gov/geo/>)

The Cancer Genome Atlas (TCGA, <https://www.cancer.gov/tcga>)

Database for Annotation, Visualization and Integrated Discovery (DAVID, <https://david.ncifcrf.gov/>),

The Search Tool for The Retrieval of Interaction Genes (STRING, <https://string-db.org/>)

Abbreviations

SCLC	Small Cell Lung Cancer
NSCLC	Non-Small Cell Lung Cancer
LUAD	Lung Adenocarcinoma
LUSC	Lung Squamous Cell Carcinoma
DEGs	Differentially Expressed Genes
PPI	Protein-protein interaction
FC	Fold Change

GEO	Gene Expression Omnibus
TCGA	The Cancer Genome Atlas
GO	Gene Ontology
KEGG	Kyoto Encyclopedia of Genes and Genomes
DAVID	Database for Annotation, Visualization and Integrated Discovery
STRING	Search Tool for The Retrieval of Interaction Genes
MCODE	Molecular Complex Detection
WGCNA	Weighted Gene Co-Expression Network Analysis
GS	Gene Significance
MM	Module Membership
OS	Overall Survival

Gene Abbreviation

RFC4	Replication Factor C Subunit 4
MAD2L1	Mitotic Arrest Deficient 2 Like 1
AURKA	Aurora Kinase A
CDKN3	Cyclin Dependent Kinase Inhibitor 3
RAD51	DNA Repair Protein RAD51 Homolog 1
TOP2A	DNA Topoisomerase II Alpha
TTK	Threonine and Tyrosine Kinase
AURKB	Aurora Kinase B
CCNA2	Cyclin A2
TPX2	Xenopus Kinesin-Like Protein 2
TK1	Thymidine Kinase 1
PBK	PDZ Binding Kinase

KPNA2	Karyopherin α 2
KIF23	Kinesin Family Member 23
KLK8	Kallikrein8
OR2W3	Olfactory Receptor Family 2 Subfamily W Member 3
H1FOO	H1.8 Linker Histone
ANKFN1	Ankyrin Repeat and Fibronectin Type III Domain Containing 1

Funding

This work was supported by National key research and development program of China (2018YFA0900200), National Natural Science Foundation of China Grants (31771519, 31871083) and Beijing Natural Science Foundation (5182012, 7182087), the Ministry of Science and Technology of China Grant 2015CB559200. Funding for open access charge: National key research and development program of China.

Author Contributions Statement

All authors contributed to the work presented in this paper. Miaomiao Gao and Zhengwei Xie identified the research topic. Miaomiao Gao performed the selection of GEO dataset data, the screening of GEO differential expressed genes, the establishment of PPI, the GO and KEGG analysis of DEGs, drawing of differentially expressed genes and wrote relevant content. Weilaixin Kong performed the screening of TCGA differential expressed genes, WGCNA analysis, survival analysis, GO and KEGG analysis of gene modules and wrote relevant content. Zhuo Huang and Zhengwei Xie gave suggestions on the choice of experimental methods and the writing of the paper. The manuscript was reviewed and approved by all authors.

Conflicts of interest

None.

References

- [1] J. Xu, Y. Shu, T. Xu, W. Zhu, T. Qiu, J. Li, M. Zhang, J. Xu, R. Guo, K. Lu, L. Zhu, Y. Yin, Y. Gu, L. Liu, P. Liu, R. Wang, Microarray expression profiling and bioinformatics analysis of circular rna expression in lung squamous cell carcinoma, *Am. J. Transl. Res.* 10 (2018) 771-783.
- [2] L. Gao, Y.N. Guo, J.H. Zeng, F.C. Ma, J. Luo, H.W. Zhu, S. Xia, K.L. Wei, G. Chen, The expression, significance and function of cancer susceptibility candidate 9 in lung squamous cell carcinoma: A bioinformatics and in vitro investigation, *Int. J. Oncol.* 54 (2019) 1651-1664. <https://doi.org/10.3892/ijo.2019.4758>.
- [3] W.J. Chen, R.X. Tang, R.Q. He, D.Y. Li, L. Liang, J.H. Zeng, X.H. Hu, J. Ma, S.K. Li, G. Chen, Clinical roles of the aberrantly expressed lncRNAs in lung squamous cell carcinoma: A study based on RNA sequencing and microarray data mining, *Oncotarget* 8 (2017) 61282-61304. <https://doi.org/10.18632/oncotarget.18058>.
- [4] C.H.Y. Cheung, H.F. Juan, Quantitative proteomics in lung cancer, *J. Biomed. Sci.* 24 (2017) 37. <https://doi.org/10.1186/s12929-017-0343-y>.
- [5] Y. Zhang, Q. Yang, S. Wang, MicroRNAs: A new key in lung cancer, *Cancer Chemother. Pharmacol.* 74 (2014) 1105-1111. <https://doi.org/10.1007/s00280-014-2559-9>.
- [6] F. Oberndorfer, L. Müllauer, Molecular pathology of lung cancer: Current status and perspectives, *Curr. Opin. Oncol.* 30 (2018) 69-76. <https://doi.org/10.1097/CCO.0000000000000429>.
- [7] B. Piperdi, A. Merla, R. Perez-Soler, Targeting angiogenesis in squamous non-small cell

- lung cancer, *Drugs* 74 (2014) 403-413. <https://doi.org/10.1007/s40265-014-0182-z>.
- [8] K.H. Yu, C. Zhang, G.J. Berry, R.B. Altman, C. R  D.L. Rubin, M. Snyder, Predicting non-small cell lung cancer prognosis by fully automated microscopic pathology image features, *Nat. Commun.* 7 (2016) 12474. <https://doi.org/10.1038/ncomms12474>.
- [9] L. Qian, L. Lin, Y. Du, X. Hao, Y. Zhao, X. Liu, MicroRNA-588 suppresses tumor cell migration and invasion by targeting GRN in lung squamous cell carcinoma, *Mol. Med. Rep.* 14 (2016) 3021-3028. <https://doi.org/10.3892/mmr.2016.5643>.
- [10] Y. Mao, D. Yang, J. He, M.J. Krasna, Epidemiology of lung cancer, *Surg. Oncol. Clin. N. Am.* 25 (2016) 439-445. <https://doi.org/10.1016/j.soc.2016.02.001>.
- [11] Q. Wang, S. Liu, X. Zhao, Y. Wang, D. Tian, W. Jiang, MiR-372-3p promotes cell growth and metastasis by targeting FGF9 in lung squamous cell carcinoma, *Cancer Med.* 6 (2017) 1323-1330. <https://doi.org/10.1002/cam4.1026>.
- [12] Y. Matsuoka, Y. Takagi, K. Nosaka, T. Sakabe, T. Haruki, K. Araki, Y. Taniguchi, T. Shiomi, H. Nakamura, Y. Umekita, Cytoplasmic expression of maspin predicts unfavourable prognosis in patients with squamous cell carcinoma of the lung, *Histopathology* 69 (2016) 114-120. <https://doi.org/10.1111/his.12921>.
- [13] F. Guo, K. Hiroshima, D. Wu, M. Satoh, M. Abulazi, I. Yoshino, T. Tomonaga, F. Nomura, Y. Nakatani, Prohibitin in squamous cell carcinoma of the lung: Its expression and possible clinical significance, *Hum. Pathol.* 43 (2012) 1282-1288. <https://doi.org/10.1016/j.humpath.2011.10.006>.
- [14] R. Edgar, M. Domrachev, A.E. Lash, Gene Expression Omnibus: NCBI gene expression and hybridization array data repository, *Nucleic Acids Res.* 30 (2002) 207-210. <https://doi.org/10.1093/nar/30.1.207>.
- [15] T. Barrett, S.E. Wilhite, P. Ledoux, C. Evangelista, I.F. Kim, M. Tomashevsky, K.A. Marshall, K.H. Phillippy, P.M. Sherman, M. Holko, A. Yefanov, H. Lee, N. Zhang, C.L.

- Robertson, N. Serova, S. Davis, A. Soboleva, NCBI GEO: Archive for functional genomics data sets – Update, *Nucleic Acids Res.* 41 (2013) D991-D995.
<https://doi.org/10.1093/nar/gks1193>.
- [16]K. Song, L. Li, G. Zhang, Bias and correction in RNA-seq data for marine species, *Mar. Biotechnol. (NY)* 19 (2017) 541-550. <https://doi.org/10.1007/s10126-017-9773-5>.
- [17]E.A. Gehan, A generalized Wilcoxon test for comparing arbitrarily singly-censored samples, *Biometrika* 52 (1965) 203-223. <https://doi.org/10.2307/2333825>.
- [18]Gene Ontology Consortium, The Gene Ontology (GO) database and informatics resource, *Nucleic Acids Res.* 32 (2004) D258-D261. <https://doi.org/10.1093/nar/gkh036>.
- [19]H. Ogata, S. Goto, K. Sato, W. Fujibuchi, H. Bono, M. Kanehisa, KEGG: Kyoto encyclopedia of genes and genomes, *Nucleic Acids Res.* 27 (1999) 29-34.
<https://doi.org/10.1093/nar/27.1.29>.
- [20]D.W. Huang, B.T. Sherman, R.A. Lempicki, Systematic and integrative analysis of large gene lists using DAVID bioinformatics resources, *Nat. Protoc.* 4 (2009) 44-57.
<https://doi.org/10.1038/nprot.2008.211>.
- [21]D.W. Huang, B.T. Sherman, R.A. Lempicki, Bioinformatics enrichment tools: Paths toward the comprehensive functional analysis of large gene lists, *Nucleic Acids Res.* 37 (2009) 1-13. <https://doi.org/10.1093/nar/gkn923>.
- [22]D. Szklarczyk, A.L. Gable, D. Lyon, A. Junge, S. Wyder, J. Huerta-Cepas, M. Simonovic, N.T. Doncheva, J.H. Morris, P. Bork, L.J. Jensen, C.V. Mering, STRING v11: Protein-protein association networks with increased coverage, supporting functional discovery in genome-wide experimental datasets, *Nucleic Acids Res.* 47 (2019) D607-D613. <https://doi.org/10.1093/nar/gky1131>.
- [23]P. Shannon, A. Markiel, O. Ozier, N.S. Baliga, J.T. Wang, D. Ramage, N. Amin, B. Schwikowski, T. Ideker, Cytoscape: A software Environment for integrated models of

biomolecular interaction networks, *Genome Res.* 13 (2003) 2498-2504.

<https://doi.org/10.1101/gr.1239303>.

[24] G.D. Bader, C.W.V. Hogue, An automated method for finding molecular complexes in large protein interaction networks, *BMC Bioinformatics* 4 (2003) 2.

<https://doi.org/10.1186/1471-2105-4-2>.

[25] B. Zhang, S. Horvath, A general framework for weighted gene co-expression network analysis, *Stat. Appl. Genet. Mol. Biol.* 4 (2005) Article 17. <https://doi.org/10.2202/1544-6115.1128>.

[26] P. Langfelder, S. Horvath, WGCNA: An R package for weighted correlation network analysis, *BMC Bioinformatics* 9 (2008) 559. <https://doi.org/10.1186/1471-2105-9-559>.

[27] M. Lunn, D. McNeil, Applying Cox regression to competing risks, *Biometrics* 51 (1995) 524-532. <https://doi.org/10.2307/2532940>.

[28] H.R. Shahraki, A. Salehi, N. Zare, Survival prognostic factors of male breast cancer in Southern Iran: A LASSO-Cox regression approach, *Asian Pacific J. Cancer Prev.* 16 (2015) 6773-6777. <https://doi.org/10.7314/APJCP.2015.16.15.6773>.

[29] H. Liang, X.S. Hao, P. Wang, X.N. Wang, J.W. Li, J.C. Wang, D.C. Wang, Multivariate Cox analysis on prognostic factors after surgery for rectal carcinoma, *Zhonghua Zhong Liu Za Zhi*, 26 (2004) 688-691. (in Chinese)

[30] R. Huang, X. Liao, Q. Li, Identification and validation of potential prognostic gene biomarkers for predicting survival in patients with acute myeloid leukemia, *Oncotargets Ther.* 10 (2017) 5243-5254. <https://doi.org/10.2147/OTT.S147717>.

[31] M. Schemper, R. Henderson, Predictive accuracy and explained variation in Cox regression, *Biometrics* 56 (2000) 249-255. <https://doi.org/10.1111/j.0006-341X.2000.00249.x>.

[32] J.D. Morrow, X. Zhou, T. Lao, Z. Jiang, D.L. DeMeo, M.H. Cho, W. Qiu, S. Cloonan, V.

- Pinto-Plata, B. Celli, N. Marchetti, G.J. Criner, R. Bueno, G.R. Washko, K. Glass, J. Quackenbush, A.M. Choi, E.K. Silverman, C.P. Hersh, Functional interactors of three genome-wide association study genes are differentially expressed in severe chronic obstructive pulmonary disease lung tissue, *Sci. Rep.* 7 (2017) 44232.
<https://doi.org/10.1038/srep44232>.
- [33] T.S. Mok, Y.L. Wu, S. Thongprasert, C.H. Yang, D.T. Chu, N. Saijo, P. Sunpaweravong, B. Han, B. Margono, Y. Ichinose, Y. Nishiwaki, Y. Ohe, J.J. Yang, B. Chewaskulyong, H. Jiang, E.L. Duffield, C.L. Watkins, A.A. Armour, M. Fukuoka, Gefitinib or carboplatin-paclitaxel in pulmonary adenocarcinoma, *N. Engl. J. Med.* 361 (2009) 947-957. <https://doi.org/10.1056/NEJMoa0810699>.
- [34] J.R. Germ á A.F. Sagarra, M.A. Izquierdo, M.A. Segu í Sequential trials of cisplatin, vinblastine, and bleomycin and etoposide and cisplatin in disseminated nonseminomatous germ cell tumors of the testis with a good prognosis at a single institution, *Cancer* 71 (1993) 796-803. [https://doi.org/10.1002/1097-0142\(19930201\)71:3<796::AID-CNCR2820710323>3.0.CO;2-1](https://doi.org/10.1002/1097-0142(19930201)71:3<796::AID-CNCR2820710323>3.0.CO;2-1).
- [35] M. Yan, C. Wang, B. He, M. Yang, M. Tong, Z. Long, B. Liu, F. Peng, L. Xu, Y. Zhang, D. Liang, H. Lei, S. Subrata, K.W. Kelley, E.W. Lam, B. Jin, Q. Liu, Aurora-A Kinase: A potent oncogene and target for cancer therapy, *Med. Res. Rev.* 36 (2016) 1036-1079.
<https://doi.org/10.1002/med.21399>.
- [36] T. Kato, H. Wada, P. Patel, H.P. Hu, D. Lee, H. Ujiie, K. Hirohashi, T. Nakajima, M. Sato, M. Kaji, K. Kaga, Y. Matsui, M.S. Tsao, K. Yasufuku, Overexpression of KIF23 predicts clinical outcome in primary lung cancer patients, *Lung Cancer* 92 (2016) 53-61.
<https://doi.org/10.1016/j.lungcan.2015.11.018>.
- [37] B. Budke, W. Lv, A.P. Kozikowski, P.P. Connell, Recent developments using small molecules to target RAD51: How to best modulate RAD51 for anticancer therapy?,

- ChemMedChem 11 (2016) 2468-2473. <https://doi.org/10.1002/cmdc.201600426>.
- [38] R. Dachineni, G. Ai, D.R. Kumar, S.S. Sadhu, H. Tummala, G.J. Bhat, Cyclin A2 and CDK2 as novel targets of aspirin and salicylic acid: A potential role in cancer prevention, Mol. Cancer Res. 14 (2016) 241-252. <https://doi.org/10.1158/1541-7786.MCR-15-0360>.
- [39] A. Christiansen, L. Dyrskjøl, The functional role of the novel biomarker karyopherin α 2 (KPNA2) in cancer, Cancer Lett. 331 (2013) 18-23. <https://doi.org/10.1016/j.canlet.2012.12.013>.
- [40] Y. Xie, A. Wang, J. Lin, L. Wu, H. Zhang, X. Yang, X. Wan, R. Miao, X. Sang, H. Zhao, Mps1/TTK: a novel target and biomarker for cancer, J. Drug Target 25 (2017) 112-118. <https://doi.org/10.1080/1061186X.2016.1258568>.
- [41] T. Otto, P. Sicinski, Cell cycle proteins as promising targets in cancer therapy, Nat. Rev. Cancer 17 (2017) 93-115. <https://doi.org/10.1038/nrc.2016.138>.
- [42] Y. Liao, Y. Liao, J. Li, J. Li, Y. Fan, B. Xu, Polymorphisms in *AURKA* and *AURKB* are associated with the survival of triple-negative breast cancer patients treated with taxane-based adjuvant chemotherapy, Cancer Manag. Res. 10 (2018) 3801-3808. <https://doi.org/10.2147/CMAR.S174735>.
- [43] Z. Yu, Y. Sun, X. She, Z. Wang, S. Chen, Z. Deng, Y. Zhang, Q. Liu, Q. Liu, C. Zhao, P. Li, C. Liu, J. Feng, H. Fu, G. Li, M. Wu, SIX3, a tumor suppressor, inhibits astrocytoma tumorigenesis by transcriptional repression of *AURKA/B*, J. Hematol. Oncol. 10 (2017) 115. <https://doi.org/10.1186/s13045-017-0483-2>.
- [44] Z.L. Ma, B.J. Zhang, D.T. Wang, X. Li, J.L. Wei, B.T. Zhao, Y. Jin, Y.L. Li, Y.X. Jin, Tanshinones suppress *AURKA* through up-regulation of miR-32 expression in non-small cell lung cancer, Oncotarget 6 (2015) 20111-20120. <https://doi.org/10.18632/oncotarget.3933>.
- [45] X. Jin, X. Liu, X. Li, Y. Guan, Integrated analysis of DNA methylation and mRNA

- expression profiles data to identify key genes in lung adenocarcinoma, *Biomed. Res. Int.* 2016 (2016) 4369431. <https://doi.org/10.1155/2016/4369431>.
- [46] S. Bhattacharya, K. Srinivasan, S. Abdisalaam, F. Su, P. Raj, I. Dozmorov, R. Mishra, E.K. Wakeland, S. Ghose, S. Mukherjee, A. Asaithamby, RAD51 interconnects between DNA replication, DNA repair and immunity, *Nucleic Acids Res.* 45 (2017) 4590-4605. <https://doi.org/10.1093/nar/gkx126>.
- [47] J. Hu, Z. Zhang, L. Zhao, L. Li, W. Zuo, L. Han, High expression of RAD51 promotes DNA damage repair and survival in KRAS-mutant lung cancer cells, *BMB Rep.* 52 (2019) 151-156. <https://doi.org/10.5483/BMBRep.2019.52.2.213>.
- [48] T. Takenaka, I. Yoshino, H. Kouso, T. Ohba, T. Yohena, A. Osoegawa, F. Shoji, Y. Maehara, Combined evaluation of Rad51 and ERCC1 expressions for sensitivity to platinum agents in non-small cell lung cancer, *Int. J. Cancer* 121 (2007) 895-900. <https://doi.org/10.1002/ijc.22738>.
- [49] S.T. Pachis, G.J.P.L. Kops, Leader of the SAC: Molecular mechanisms of Mps1/TTK regulation in mitosis, *Open Biol.* 8 (2018) 180109. <https://doi.org/10.1098/rsob.180109>.
- [50] L. Zheng, Z. Chen, M. Kawakami, Y. Chen, J. Roszik, L.M. Mustachio, J.M. Kurie, P. Villalobos, W. Lu, C. Behrens, B. Mino, L.M. Solis, J. Silvester, K.L. Thu, D.W. Cescon, J. Rodriguez-Canales, I.I. Wistuba, T.W. Mak, X. Liu, E. Dmitrovsky, Threonine tyrosine kinase inhibition eliminates lung cancers by augmenting apoptosis and polyploidy, *Mol. Cancer Ther.* 18 (2019) 1775-1786. <https://doi.org/10.1158/1535-7163.mct-18-0864>.
- [51] C.T. Cheung, N. Bendris, C. Paul, A. Hamieh, Y. Anouar, M. Hahne, J.M. Blanchard, B. Lemmers, Cyclin A2 modulates EMT via β -catenin and phospholipase C pathways, *Carcinogenesis* 36 (2015) 914-924. <https://doi.org/10.1093/carcin/bgv069>.
- [52] R. Chen, Y. Zhang, C. Zhang, H. Wu, S. Yang, miR-137 inhibits the proliferation of

- human non-small cell lung cancer cells by targeting SRC3, *Oncol. Lett.* 13 (2017) 3905-3911. <https://doi.org/10.3892/ol.2017.5904>.
- [53] B. Liang, C. Jia, Y. Huang, H. He, J. Li, H. Liao, X. Liu, X. Liu, X. Bai, D. Yang, TPX2 level correlates with hepatocellular carcinoma cell proliferation, apoptosis, and EMT, *Dig. Dis. Sci.* 60 (2015) 2360-2372. <https://doi.org/10.1007/s10620-015-3730-9>.
- [54] D.M. Lin, Y. Ma, T. Xiao, S.P. Guo, N.J. Han, K. Su, S.Z. Yi, J. Fang, S.J. Cheng, Y.N. Gao, TPX2 expression and its significance in squamous cell carcinoma of lung, *Zhonghua Bing Li Xue Za Zhi* 35 (2006) 540-544. (in Chinese)
- [55] G. Garrido, I. Vernos, Non-centrosomal TPX2-dependent regulation of the Aurora a kinase: Functional implications for healthy and pathological cell division, *Front. Oncol.* 6 (2016) 88. <https://doi.org/10.3389/fonc.2016.00088>.
- [56] M.A. Schneider, P. Christopoulos, T. Muley, A. Warth, U. Klingmueller, M. Thomas, F.J. Herth, H. Dienemann, N.S. Mueller, F. Theis, M. Meister, AURKA, DLGAP5, TPX2, KIF11 and CKAP5: Five specific mitosis-associated genes correlate with poor prognosis for non-small cell lung cancer patients, *Int. J. Oncol.* 50 (2017) 365-372. <https://doi.org/10.3892/ijo.2017.3834>.
- [57] L.N. Zhou, Y. Tan, P. Li, P. Zeng, M.B. Chen, Y. Tian, Y.Q. Zhu, Prognostic value of increased KPNA2 expression in some solid tumors: A systematic review and meta-analysis, *Oncotarget* 8 (2017) 303-314. <https://doi.org/10.18632/oncotarget.13863>.
- [58] C.I. Wang, C.L. Wang, C.W. Wang, C.D. Chen, C.C. Wu, Y. Liang, Y.H. Tsai, Y.S. Chang, J.S. Yu, C.J. Yu, Importin subunit alpha-2 is identified as a potential biomarker for non-small cell lung cancer by integration of the cancer cell secretome and tissue transcriptome, *Int. J. Cancer* 128 (2011) 2364-2372. <https://doi.org/10.1002/ijc.25568>.
- [59] A.L. Vikberg, T. Vooder, K. Lokk, T. Annilo, I. Golovleva, Mutation analysis and copy number alterations of KIF23 in non-small-cell lung cancer exhibiting KIF23 over-

expression, *Onco. Targets Ther.* 10 (2017) 4969-4979.

<https://doi.org/10.2147/OTT.S138420>.

[60] L. Sun, C. Zhang, Z. Yang, Y. Wu, H. Wang, Z. Bao, T. Jiang, KIF23 is an independent prognostic biomarker in glioma, transcriptionally regulated by TCF-4, *Oncotarget* 7 (2016) 24646-24655. <https://doi.org/10.18632/oncotarget.8261>.

[61] F. Iltzsche, K. Simon, S. Stopp, G. Pattschull, S. Francke, P. Wolter, S. Hauser, D.J. Murphy, P. Garcia, A. Rosenwald, S. Gaubatz, An important role for Myb-MuvB and its target gene KIF23 in a mouse model of lung adenocarcinoma, *Oncogene* 36 (2017) 110-121. <https://doi.org/10.1038/onc.2016.181>.

[62] K. Väik, T. Vooder, R. Kolde, M.A. Reintam, C. Petzold, J. Vilo, A. Metspalu, Gene expression profiles of non-small cell lung cancer: Survival prediction and new biomarkers, *Oncology* 79 (2011) 283-292. <https://doi.org/10.1159/000322116>.

[63] L. Ye, H.J. Li, F. Zhang, T.F. Lv, H.B. Liu, Y. Song, Expression of KIF23 and its prognostic role in non-small cell lung cancer: Analysis based on the data-mining of oncomine, *Zhongguo Fei Ai Za Zhi* 20 (2017) 822-826. <https://doi.org/10.3779/j.issn.1009-3419.2017.12.05>. (in Chinese)

[64] M. Paliouras, E.P. Diamandis, Intracellular signaling pathways regulate hormone-dependent kallikrein gene expression, *Tumor Biol.* 29 (2008) 63-75. <https://doi.org/10.1159/000135686>.

[65] G.M. Yousef, G.M. Yacoub, M.E. Polymeris, C. Popalis, A. Soosaipillai, E.P. Diamandis, Kallikrein gene downregulation in breast cancer, *Br. J. Cancer* 90 (2004) 167-172. <https://doi.org/10.1038/sj.bjc.6601451>.

[66] C.A. Borgono, T. Kishi, A. Scorilas, N. Harbeck, J. Dorn, B. Schmalfeldt, M. Schmitt, E.P. Diamandis, Human kallikrein 8 protein (hK8) in ovarian cancer cytosols: A new marker of favorable prognosis, *Cancer Res.* 64 (2004) 1025 LP - 1025.

http://cancerres.aacrjournals.org/content/64/7_Supplement/1025.2.abstract.

[67] KLK8 kallikrein related peptidase 8 [*Homo sapiens* (human)]

<https://www.ncbi.nlm.nih.gov/gene/11202>, updated on 11-Sep-2019.

[68] N. Ahmed, J. Dorn, R. Napieralski, E. Drecol, M. Kotzsch, P. Goettig, E. Zein, S. Avril, M. Kiechle, E.P. Diamandis, M. Schmitt, V. Magdolen, Clinical relevance of kallikrein-related peptidase 6 (KLK6) and 8 (KLK8) mRNA expression in advanced serous ovarian cancer, *Biol. Chem.* 397 (2016) 1265-1276. <https://doi.org/10.1515/hsz-2016-0177>.

[69] M. Cacaci, C. Giraud, L. Leger, R. Torelli, C. Martini, B. Posteraro, V. Palmieri, M. Sanguinetti, F. Bugli, A. Hartke, Expression profiling in a mammalian host reveals the strong induction of genes encoding LysM domain-containing proteins in *Enterococcus faecium*, *Sci. Rep.* 8 (2018) 12412. <https://doi.org/10.1038/s41598-018-30882-z>.

[70] C. Gough, L. Cottret, B. Lefebvre, J.J. Bono, Evolutionary history of plant LysM receptor proteins related to root endosymbiosis, *Front. Plant Sci.* 9 (2018) 923. <https://doi.org/10.3389/fpls.2018.00923>.

[71] V. Vanhorenbeeck, P. Jacquemin, F.P. Lemaigre, G.G. Rousseau, OC-3, a novel mammalian member of the ONECUT class of transcription factors, *Biochem. Biophys. Res. Commun.* 292 (2002) 848-854. <https://doi.org/10.1006/bbrc.2002.6760>.

[72] Y. Tan, Y. Yoshida, D.E. Hughes, R.H. Costa, Increased expression of hepatocyte nuclear factor 6 stimulates hepatocyte proliferation during mouse liver regeneration, *Gastroenterology* 130 (2006) 1283-1300. <https://doi.org/10.1053/j.gastro.2006.01.010>.

[73] F. Lehner, U. Kulik, J. Klempnauer, J. Borlak, Inhibition of the liver enriched protein FOXA2 recovers HNF6 activity in human colon carcinoma and liver hepatoma cells, *PLoS One* 5 (2010) e13344. <https://doi.org/10.1371/journal.pone.0013344>.

[74] L. Ovesen, M. Sørensen, J. Hannibal, L. Allingstrup, Electrical taste detection thresholds and chemical smell detection thresholds in patients with cancer, *Cancer* 68 (1991) 2260-

2265. [https://doi.org/10.1002/1097-0142\(19911115\)68:10<2260::AID-CNCR2820681026>3.0.CO;2-W](https://doi.org/10.1002/1097-0142(19911115)68:10<2260::AID-CNCR2820681026>3.0.CO;2-W).

- [75] K. Belqaid, Y. Orrevall, J. McGreevy, E. Månsson-Brahme, W. Wismer, C. Tishelman, B.M. Bernhardson, Self-reported taste and smell alterations in patients under investigation for lung cancer, *Acta Oncol.* 53 (2014) 1405-1412.
<https://doi.org/10.3109/0284186X.2014.895035>.
- [76] S. Gao, Y.G. Chung, M.H. Parseghian, G.J. King, E.Y. Adashi, K.E. Latham, Rapid H1 linker histone transitions following fertilization or somatic cell nuclear transfer: Evidence for a uniform developmental program in mice, *Dev. Biol.* 266 (2004) 62-75.
<https://doi.org/10.1016/j.ydbio.2003.10.003>.
- [77] T. Teranishi, M. Tanaka, S. Kimoto, Y. Ono, K. Miyakoshi, T. Kono, Y. Yoshimura, Rapid replacement of somatic linker histones with the oocyte-specific linker histone H1foo in nuclear transfer, *Dev. Biol.* 266 (2004) 76-86.
<https://doi.org/10.1016/j.ydbio.2003.10.004>.
- [78] L. Gao, H. Xie, L. Dong, J. Zou, J. Fu, X. Gao, L. Ou, S. Xiang, H. Song, Gankyrin is essential for hypoxia enhanced metastatic potential in breast cancer cells, *Mol. Med. Rep.* 9 (2014) 1032-1036. <https://doi.org/10.3892/mmr.2013.1860>.
- [79] S. Dawson, H. Higashitsuji, A.J. Wilkinson, J. Fujita, R.J. Mayer, Gankyrin: a new oncoprotein and regulator of pRb and p53, *Trends Cell Biol.* 16 (2006) 229-233.
<https://doi.org/10.1016/j.tcb.2006.03.001>.
- [80] J. McIntosh, G. Dennison, J.M.P. Holly, C. Jarrett, A. Frankow, E.J. Foulstone, Z.E. Winters, C.M. Perks, IGFBP-3 can either inhibit or enhance EGF-mediated growth of breast epithelial cells dependent upon the presence of fibronectin, *J. Biol. Chem.* 285 (2010) 38788-38800. <https://doi.org/10.1074/jbc.M110.177311>.

Figure captions

Figure 1. Overview of microarray signatures. (A-D). Volcano plots of DEGs of GSE2088, GSE6044, GSE19188 and TCGA datasets. The red and blue points in the plot represent statistically significant up and down-regulated DEGs. (E). Venn diagrams of DEGs of the three GEO and one TCGA dataset.

Figure 2. GO enrichment analysis of DEGs. (A) Up-regulated genes. (B) Down-regulated genes. The y-axis shows significantly enriched GO terms, and x-axis represents significance of enrichment.

Figure 3. Protein-protein interaction network analysis of DEGs. (A) PPI network of 124 significantly differentially expressed genes. Red: up-regulated genes; Green: significantly down-regulated genes; (B) The most significant module of the PPI network. Node size is positively related to degree of expression.

Figure 4. WGCNA analysis of DEGs within the TCGA data. (A). Left panel: Abscissa: power value; ordinate: R² value after linear regression of $-\log_{10}(k)$ and $\log_{10}(P(k))$. k: connectivity of the gene nodes; P(k): probability of such a node. Horizontal line: 0.9. Right panel: Abscissa: power value; ordinate: mean connectivity of gene nodes. (B).

Interrelationship between different gene modules. Colors in the heat map represent Pearson correlation coefficients between gene modules. Expression levels of gene modules are represented by the first principal component. (C). Gene modules and phenotypes quantified using Boolean variables (1 represents occurrence, 0 represents no occurrence) were used to calculate correlation coefficients, represented as a heat map. p-values are displayed in brackets. (D). Blue, yellow and turquoise module gene correlation scatter plots. X-axis represents molecule membership, i.e. Pearson correlation coefficients of gene and module (MM). Y-axis represents the importance of the gene for the phenotype, i.e. Pearson's correlation coefficient of gene and phenotype (GS: phenotype is represented by a Boolean

variable). In the yellow, blue, turquoise modules, the upper quartile value of MM was 0.756, 0.683 and 0.708 respectively; the upper quartile value of GS was 0.431, 0.390 and 0.631, respectively.

Figure 5. Lasso regression and multivariate cox regression related results. (A). Distribution of risk scores. The abscissa is arranged in order of patient risk score, with y-axis representing risk score, with more than 10 records plotted as 10. Patient with a score less than the median is plotted in green, those equal to or greater than the median in red. (B) Distribution of duration of survival. The abscissa is arranged in order of patient risk score and ordinate representing patient survival time. (C) Heat map of gene expression levels of the most 20 significant genes. Patient risk scores increased from left to right. (D). Results of Lasso regression 1000 times 10-fold cross validation. λ was determined when partial likelihood deviance was smallest. (E). Coefficient curve. Different colored lines represent coefficient sizes of individual genes in different cases. The abscissa represents $\log(\lambda)$ and the number of coefficients (top) that are not zero under this penalty factor. (F). Survival curve for patients with different risk scores. Patients were divided into two groups according to the median survival curve score. Blue represents patients with a lower risk score. p- value <0.001.

Figure 6. (A). Forest plot for multivariate cox regression. The HR value is $e\beta$. This figure displays the 95% confidence interval for the HR value over the box plot with associated p-values. An HR of less than 1 indicates that high gene expression improves prognosis, and HR greater than 1 the opposite. (B). ROC curves for the model representing 1, 3 and 5-year predictions, from left to right, respectively. The values in brackets are the areas under the curve.

Figures

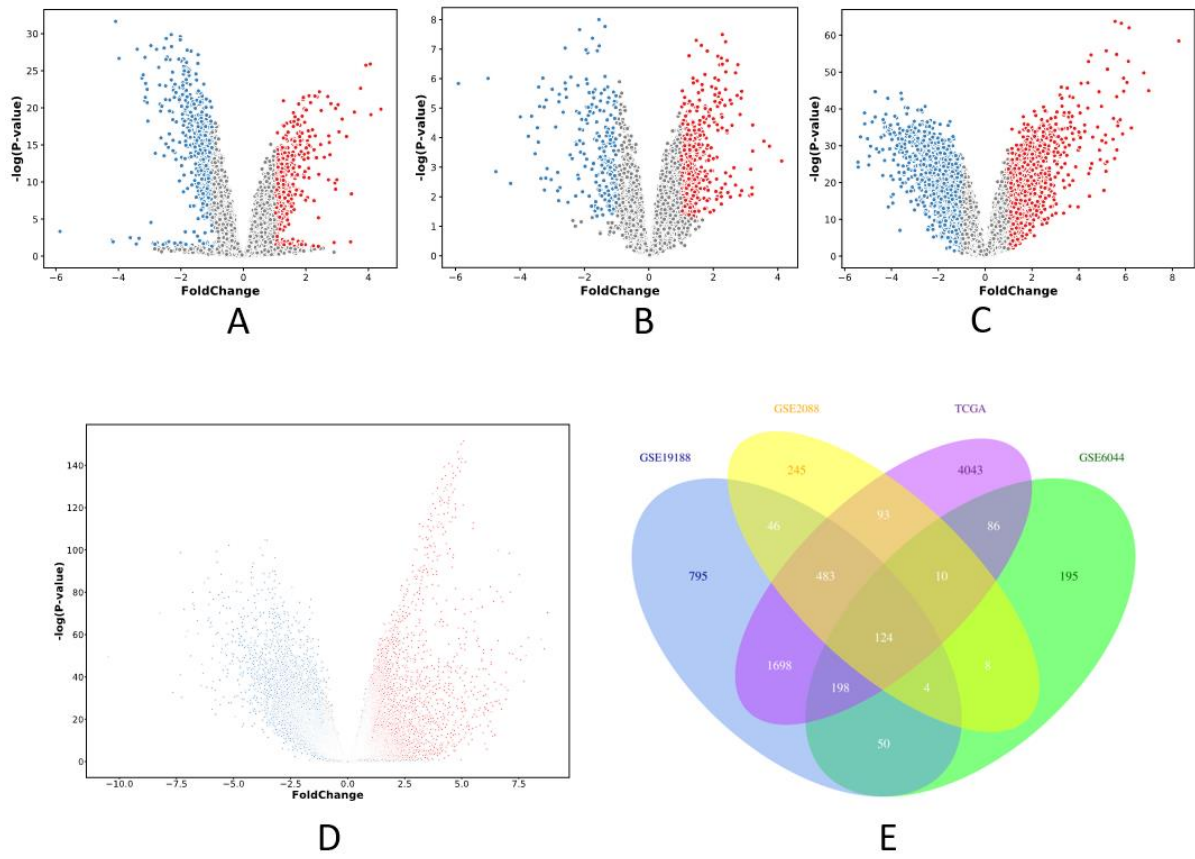


Figure 1

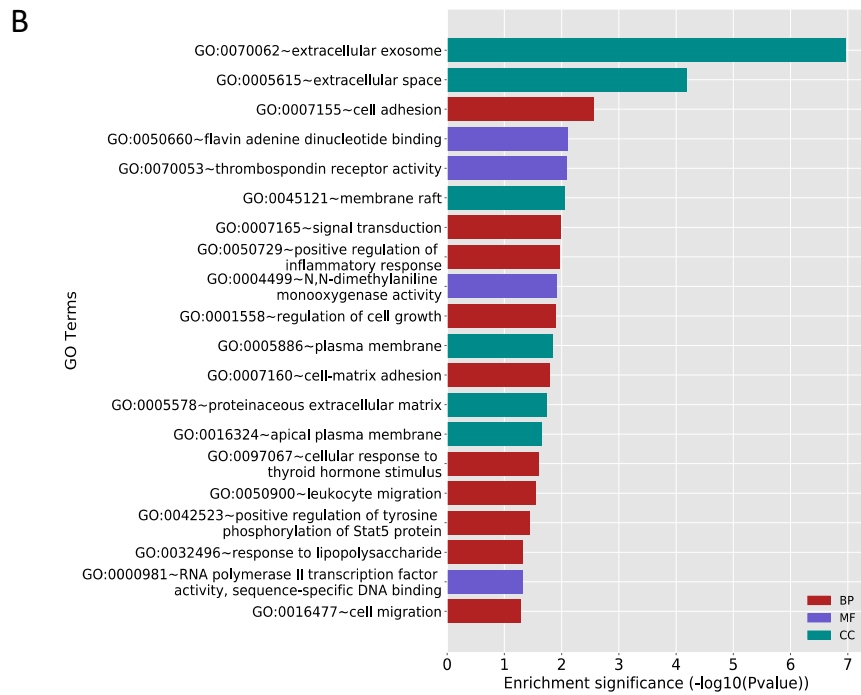
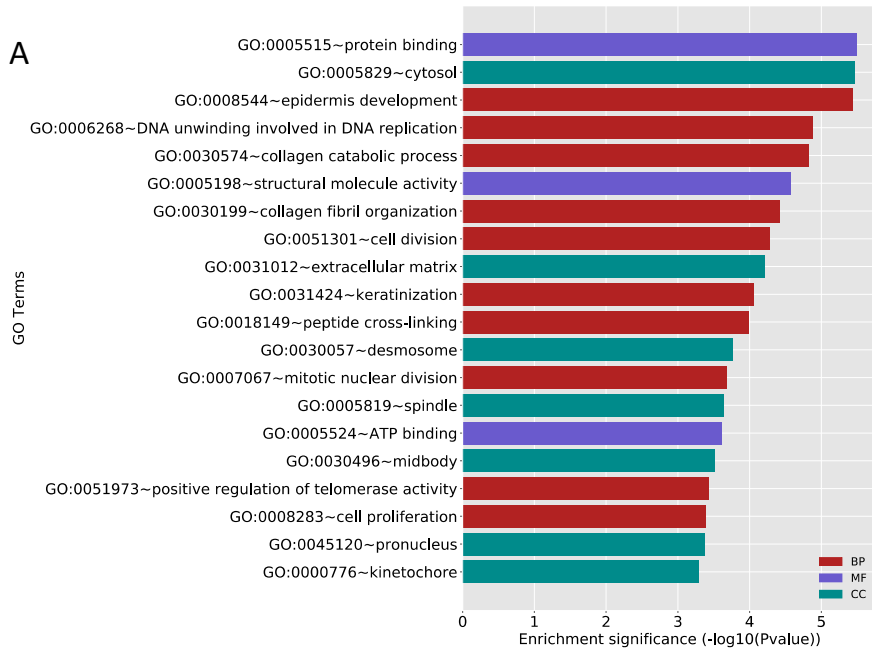


Figure 2

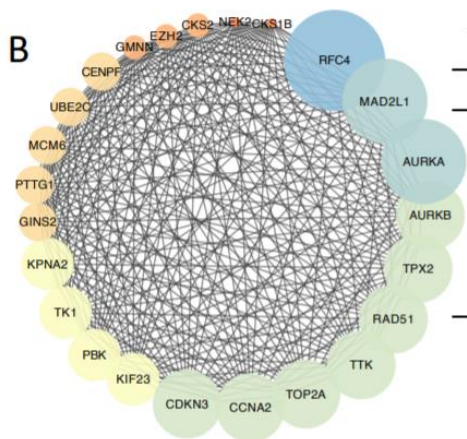
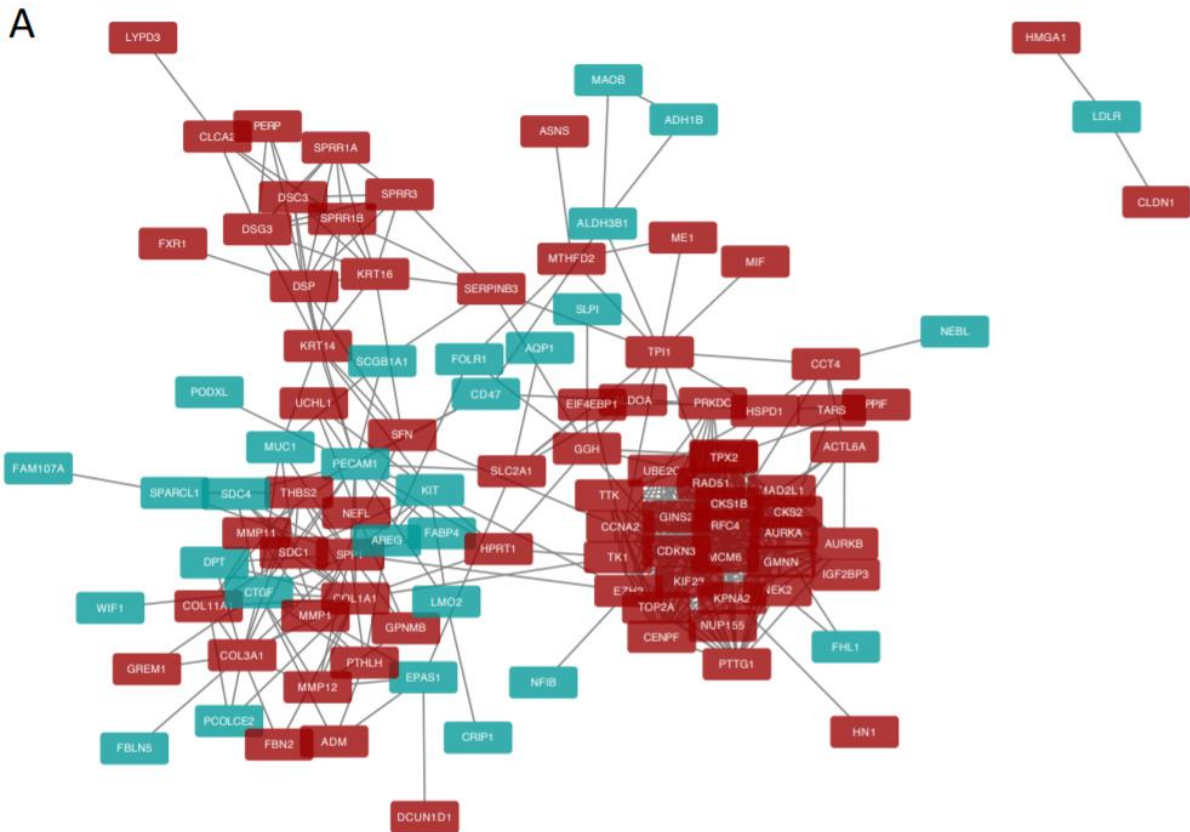


Table 1. GO term enrichment analysis of DEGs in modules.

GO Term	Count	%	Pvalue	Genes
GO:0051301*cell division	10	41.6667	4.23E-10	CKS1B, MAD2L1, NEK2, CKS2, TPX2, CENPF, AURKA, PTTG1, UBE2C, CCNA2
GO:0007067*mitotic nuclear division	8	33.3333	2.82E-08	NEK2, TPX2, CENPF, AURKA, PBK, PTTG1, AURKB, CCNA2
GO:0031145*anaphase-promoting complex-dependent catabolic process	5	20.8333	3.75E-06	MAD2L1, AURKA, PTTG1, AURKB, UBE2C
GO:0042787*protein ubiquitination involved in ubiquitin-dependent protein catabolic process	5	20.8333	5.13E-05	MAD2L1, AURKA, PTTG1, AURKB, UBE2C
GO:0006268*DNA unwinding involved in DNA replication	3	12.5	8.02E-05	TOP2A, RAD51, MCM6

Figure 3

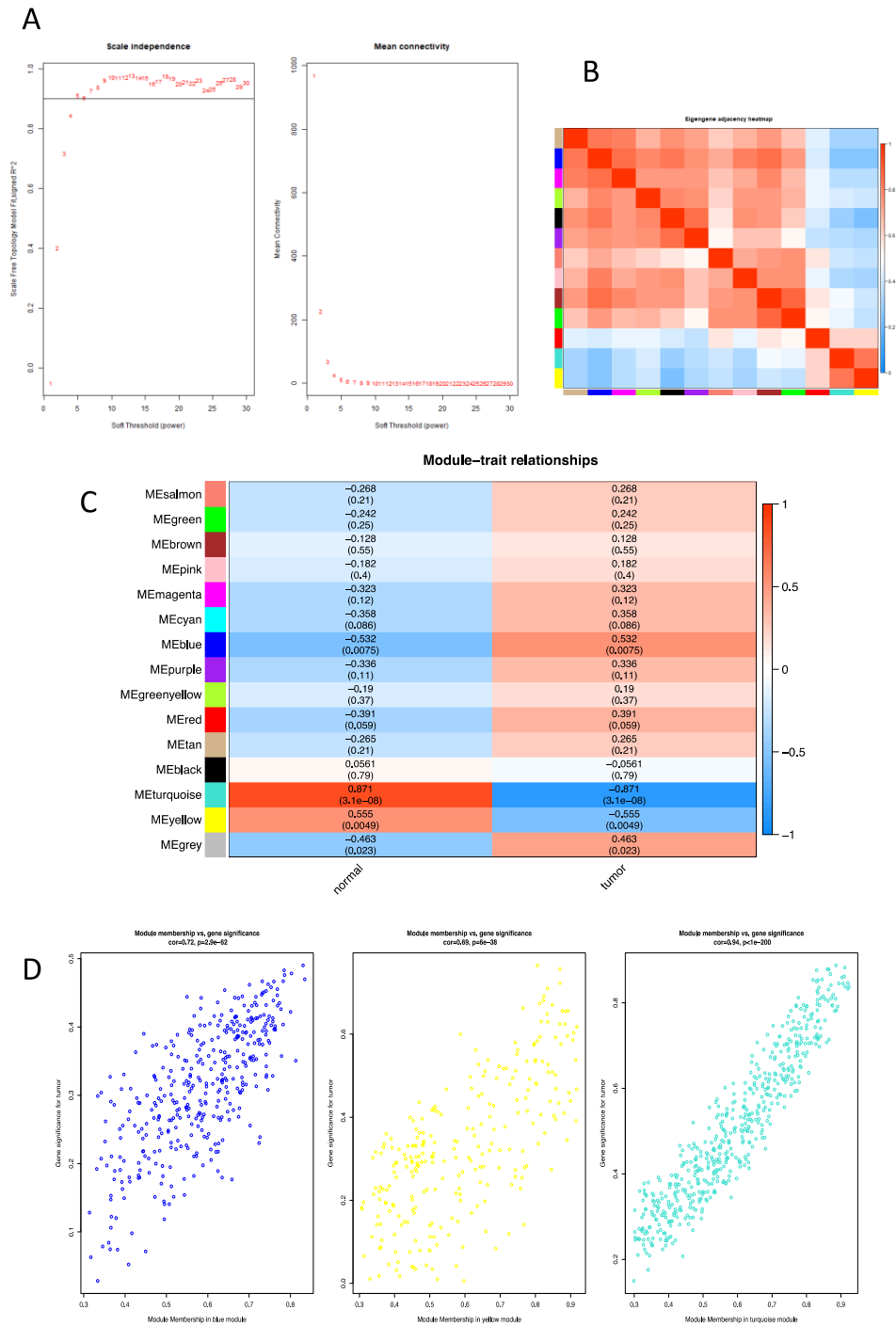


Figure 4

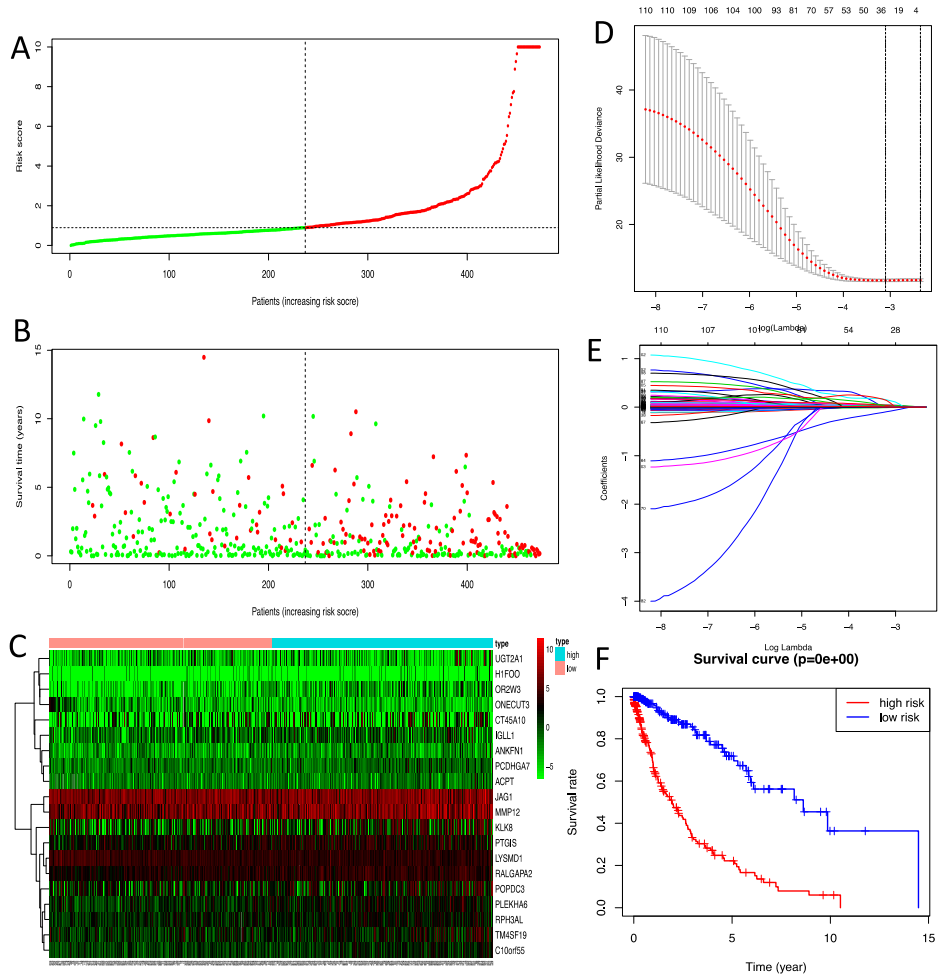


Figure 5

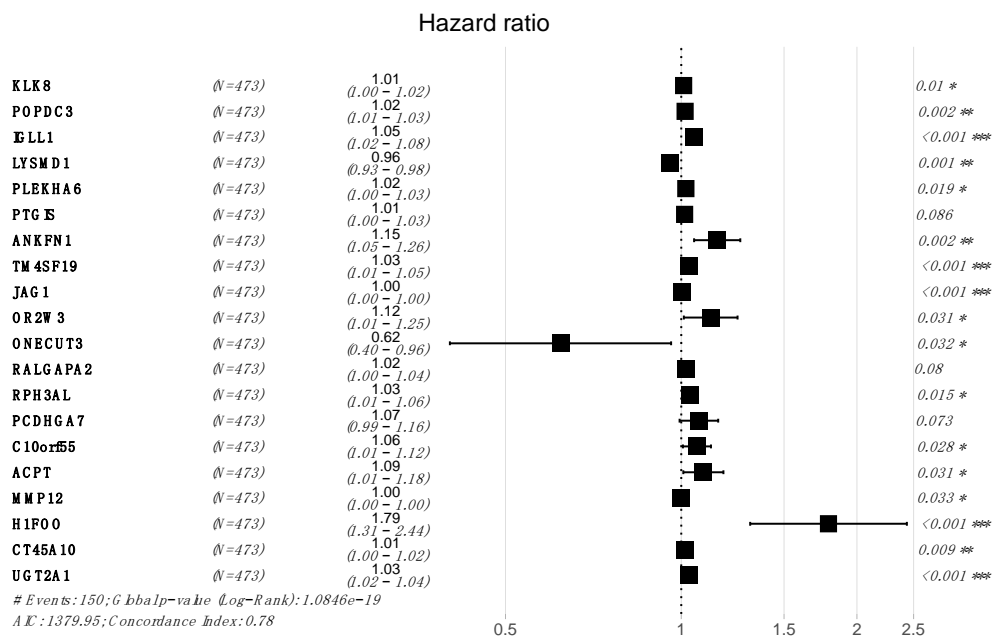


Figure 6

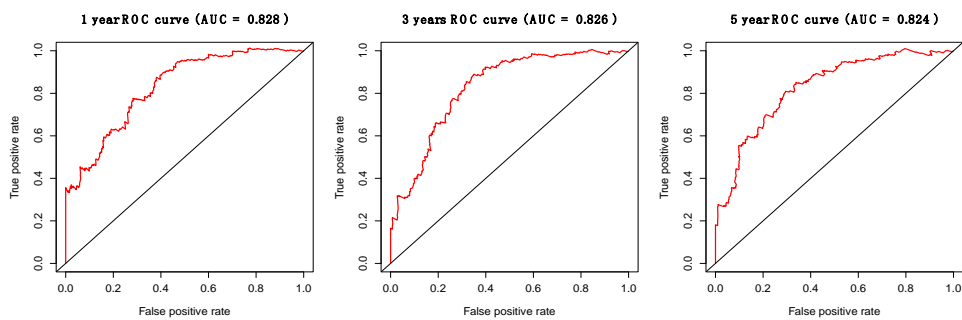


Figure 7

Supplementary materials

Table 1. Detailed information of the GEO datasets.

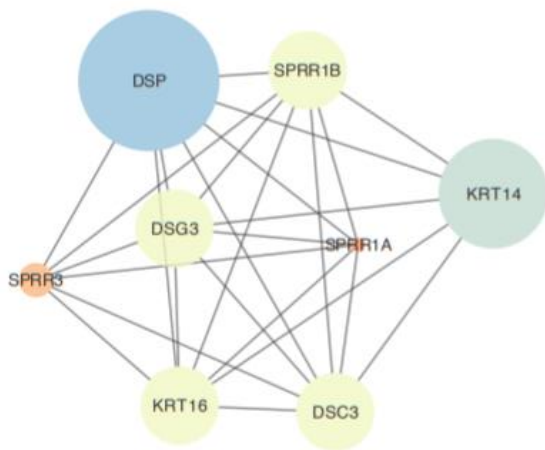
GEO Accession	Platform	Number of LUSC sample	Number of normal sample	Total
GSE2088	GPL962	48	28	76
GSE6044	GPL201	9	4	13
GSE19188	GPL570	27	65	92
In all	-	84	97	181

Table 2. KEGG pathway enrichment analysis of DEGs.

Term	Count	%	P-value	Genes
Up-regulated				
hsa04110: Cell cycle	7	8.2353	0.0002	MAD2L1, TTK, PRKDC, PTTG1, SFN, CCNA2, MCM6
hsa04512:ECM- receptor interaction	6	7.0588	0.0004	SDC1, COL3A1, COL1A1, COL11A1, THBS2, SPP1
hsa05146: Amoebiasis	4	4.7059	0.0413	COL3A1, COL1A1, SERPINB3, COL11A1
Down-regulated				
hsa00982:Drug metabolism- cytochrome P450	5	0.0872	3.03E-05	FMO5, FMO3, MAOB, ADH1B, ALDH3B1
hsa00350:Tyrosine metabolism	3	0.0523	0.0041	MAOB, ADH1B, ALDH3B1
hsa00360: Phenylalanine metabolism	2	0.0349	0.0460	MAOB, ALDH3B1

Table 3. MM and GS scores of eight significant genes.

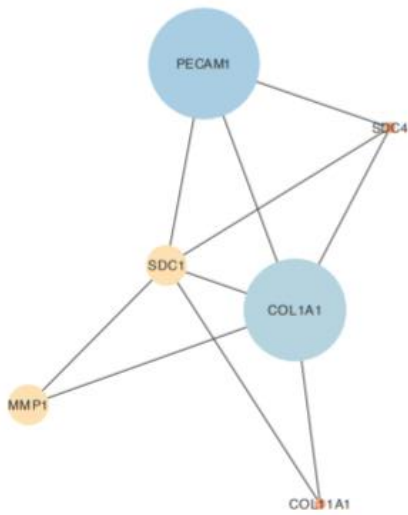
	AURKA	CCNA2	TPX2	TTK	AURKB	RAD51	KIF23	KPNA2
MM	0.732	0.699	0.69	0.738	0.7	0.74	0.8	0.776
GS	0.469	0.445	0.398	0.412	0.43	0.475	0.5	0.461



Cluster 2

MCODE score = 7.429

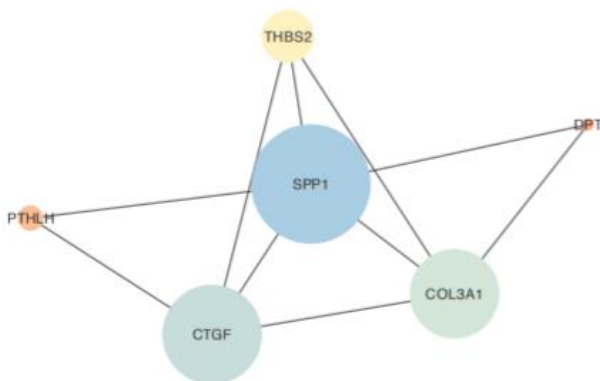
8 nodes 26 edges



Cluster 3

MCODE score = 4.0

6 nodes 10 edges



Cluster 4

MCODE score = 4.0

6 nodes 10 edges

Figure 1. The other three cluster in PPI network.

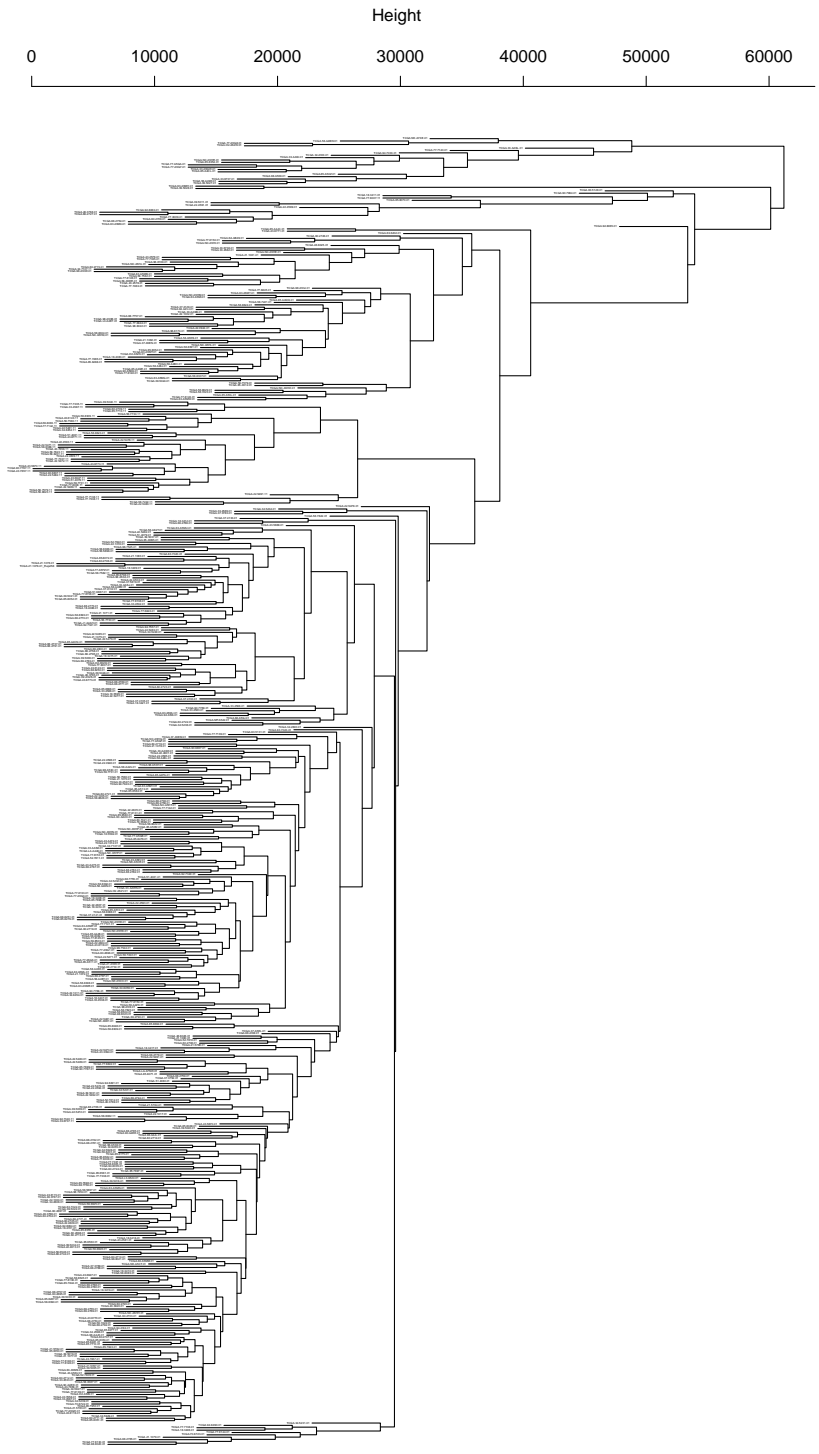
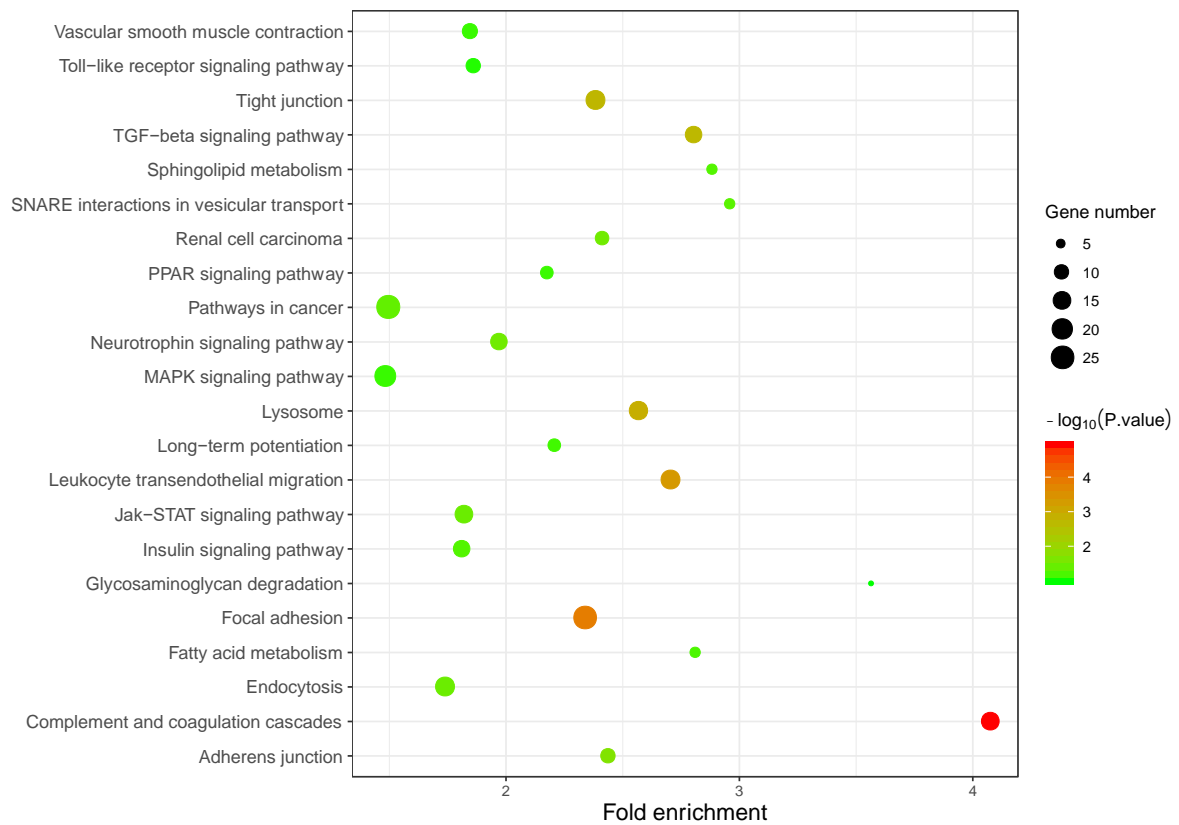
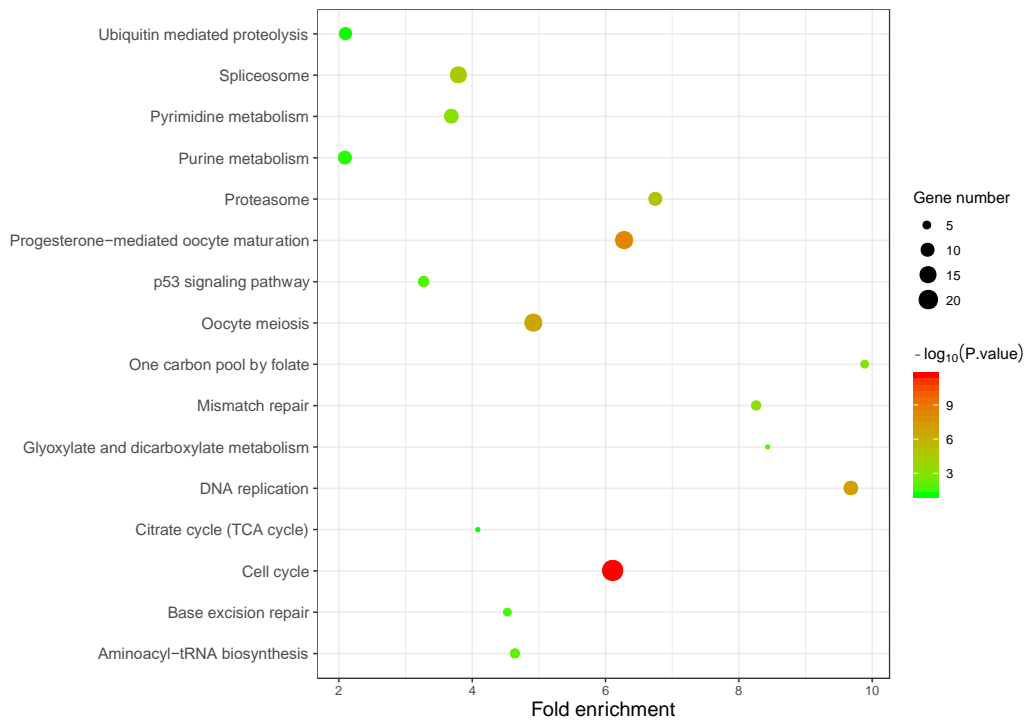


Figure 2. A tree diagram of the hierarchical clustering results before the sample is removed.



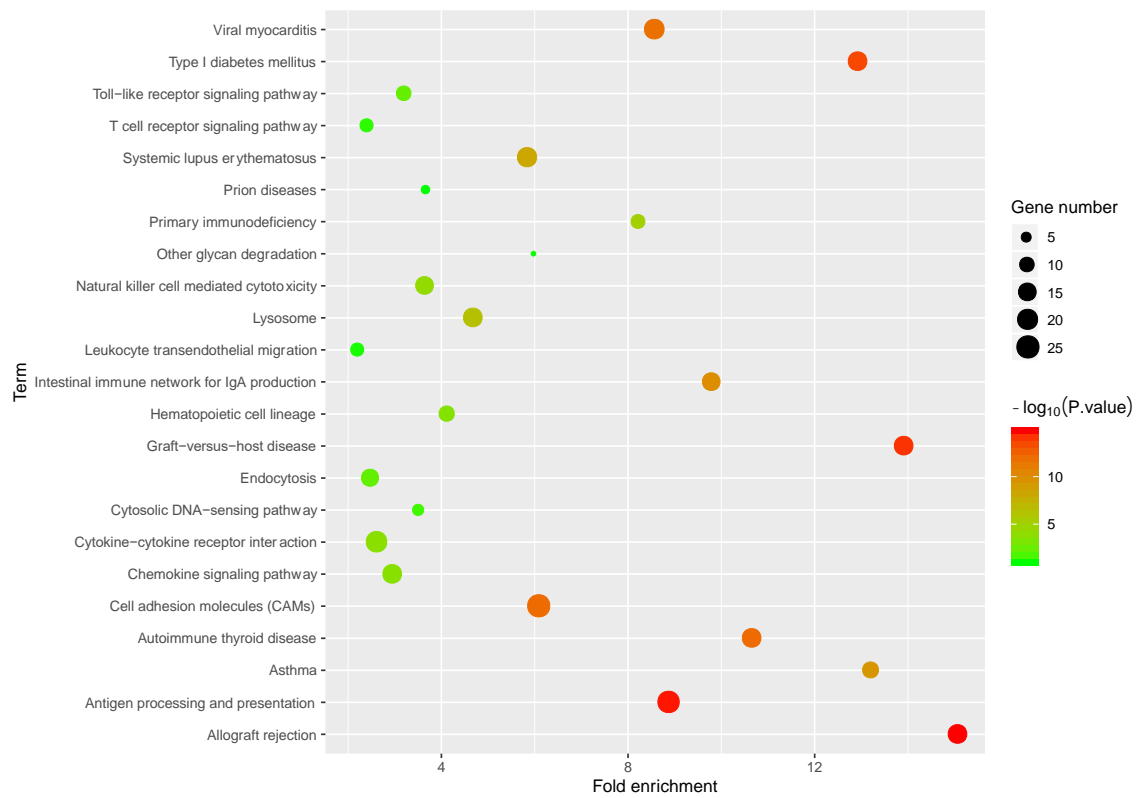
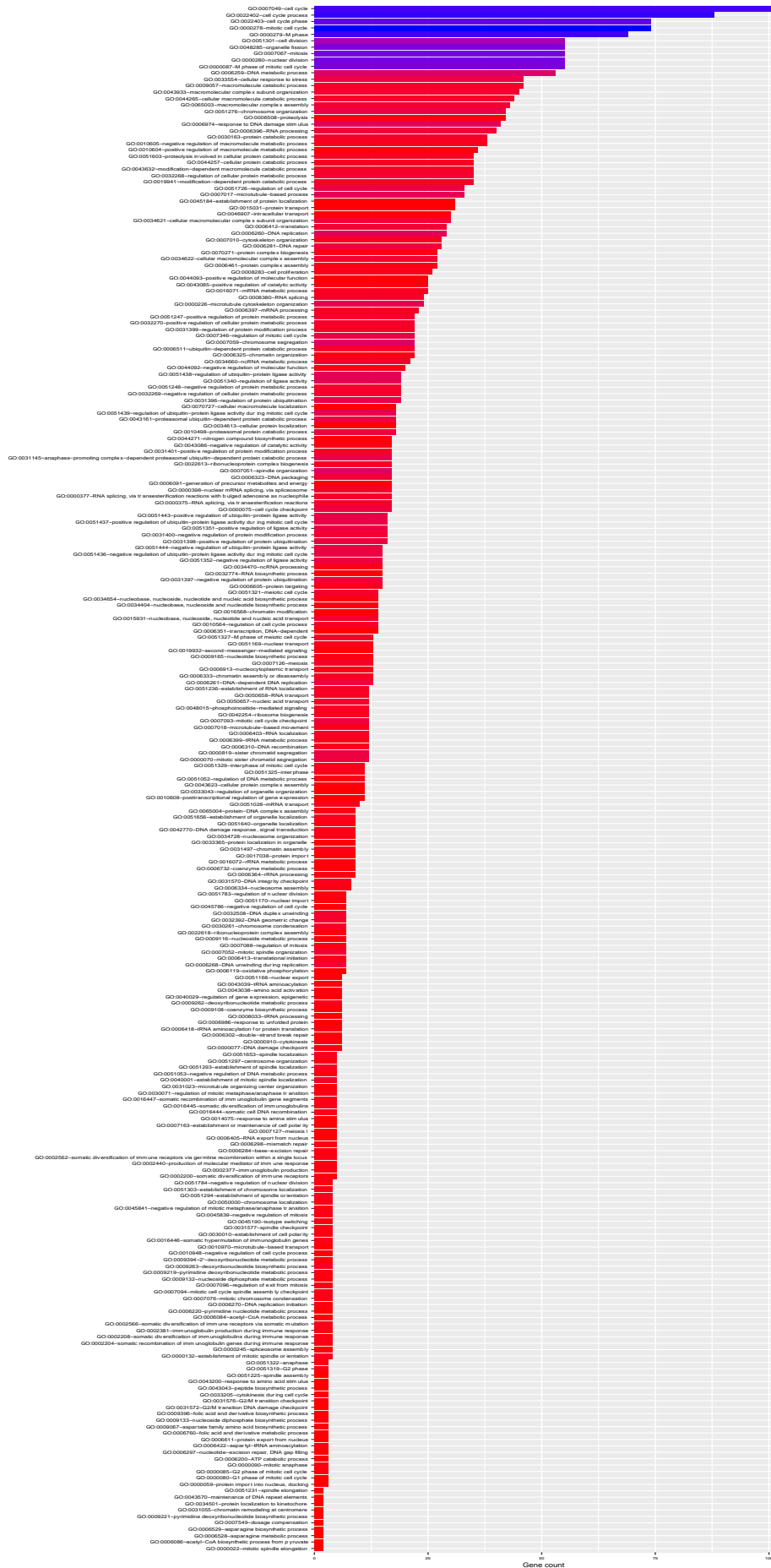


Figure3. The bubble figure of the three gene modules KEGG pathway analysis. Top, middle and bottom are the results of blue, turquoise and yellow respectively. The bubble size is the number of genes, and the bubble color represents the magnitude of the significance. The abscissa is the degree of enrichment, and the ordinate is the different regulatory pathway items.



Gene count

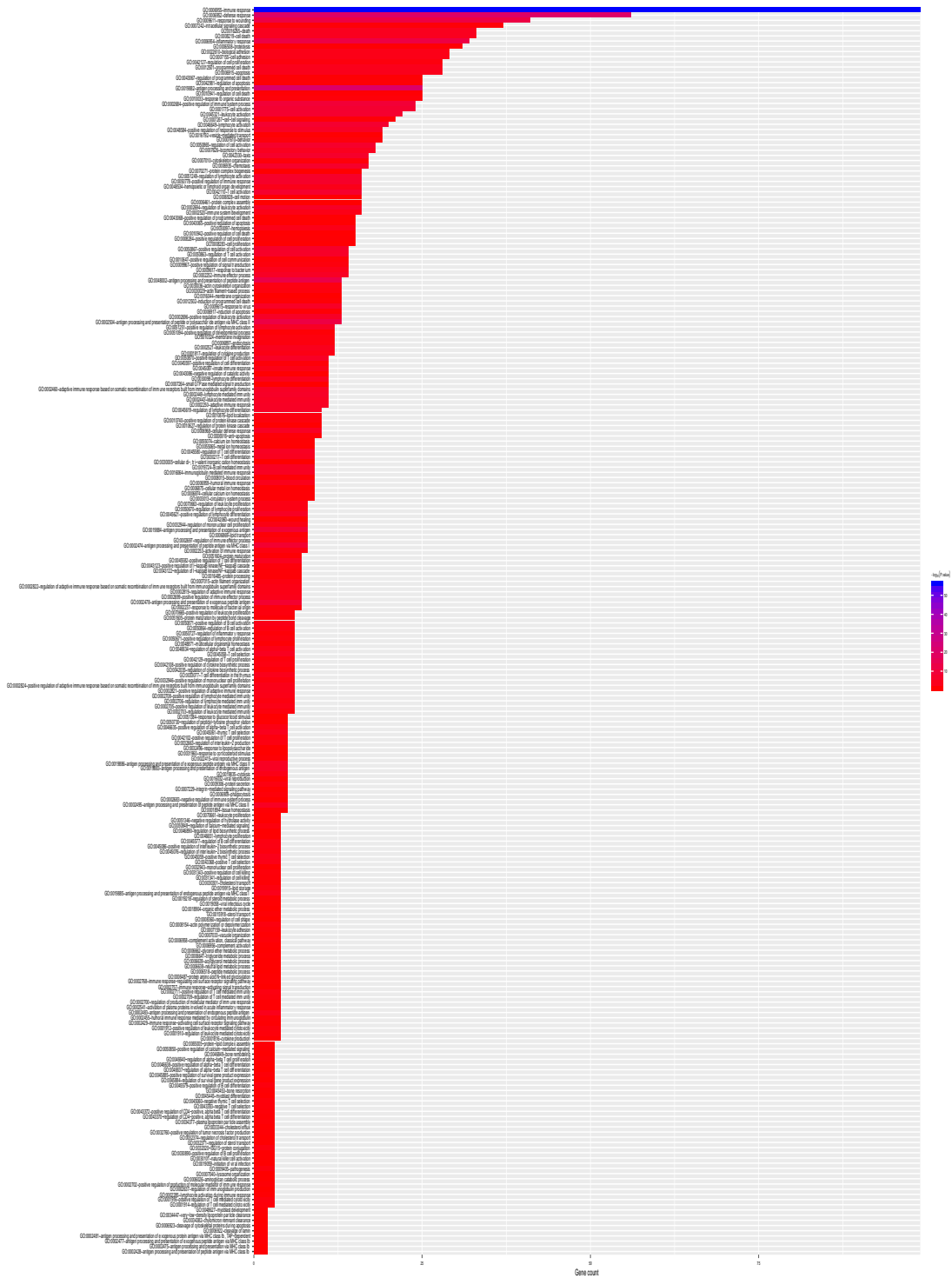


Figure 4. The figure of the three gene modules GO analysis. Top, middle and bottom are the results of blue, turquoise and yellow respectively. The y-axis shows significantly enriched GO terms, and x-axis represents significance of enrichment.